CANCER

Deficiency in mammalian STN1 promotes colon cancer development via inhibiting DNA repair

Dinh Duc Nguyen[1]†, Eugene Kim[1]†, Nhat Thong Le[2], Xianzhong Ding[3], Rishi Kumar Jaiswal[1], Raymond Joseph Kostlan[1], Thi Ngoc Thanh Nguyen[1], Olga Shiva[4], Minh Thong Le[2], Weihang Chai[1]*

Despite the high lethality of colorectal cancers (CRCs), only a limited number of genetic risk factors are identified. The mammalian ssDNA-binding protein complex CTC1-STN1-TEN1 protects genome stability, yet its role in tumorigenesis is unknown. Here, we show that attenuated CTC1/STN1 expression is common in CRCs. We generated an inducible STN1 knockout mouse model and found that STN1 deficiency in young adult mice increased CRC incidence, tumor size, and tumor load. CRC tumors exhibited enhanced proliferation, reduced apoptosis, and elevated DNA damage and replication stress. We found that STN1 deficiency down-regulated multiple DNA glycosylases, resulting in defective base excision repair (BER) and accumulation of oxidative damage. Collectively, this study identifies STN1 deficiency as a risk factor for CRC and implicates the previously unknown STN1-BER axis in protecting colon tissues from oxidative damage, therefore providing insights into the CRC tumor–suppressing mechanism.

INTRODUCTION

Colorectal cancer (CRC) is the third most common cancer and one of the most lethal cancers worldwide (*1*). CRC cases are escalating in young adults (*2*), underscoring the need to understand its etiologic causes. CRC may take more than a decade to develop in continuous stages from polyps to adenocarcinoma (*3*). This long progression provides an intervention opportunity to prevent it from developing into advanced cancer. Identifying CRC risk factors and understanding the mechanism of CRC development are crucial to CRC treatment and prevention.

Both genetic and environmental factors are strongly associated with increased risks for CRC, albeit not fully understood (*4*, *5*). Individuals having healthy lifestyles can still develop CRCs, suggesting that genetic factors play a substantial role in CRC susceptibility. While ~30% of CRC patients have a family history of the disease, only ~5% harbor germline mutations, including mismatch repair (MMR) gene mutations in Lynch syndrome patients, *APC* mutations in familial adenomatous polyposis, *MUTYH* mutations in MUTYH-associated polyposis, *BRCA1/2* mutations, and others. The remaining 25% of patients have unidentified genetic conditions (*6*).

Genomic instability appears to be a key molecular and pathogenic factor that occurs in the initiation process of CRCs (*7*–*9*). Although recent studies using The Cancer Genome Atlas (TCGA) database have identified mutations associated with DNA damage response/repair genes in CRC and putative driver mutations have been identified (*10*–*12*), very few are validated with in vivo studies. The mechanism that influences genomic stability in CRC is unclear and remains to be determined.

[1]Department of Cancer Biology, Cardinal Bernardin Cancer Center, Loyola University Chicago Stritch School of Medicine, Maywood, IL, USA. [2]School of Biotechnology, International University, Ho Chi Minh City, Vietnam. [3]Department of Pathology, Loyola University Chicago Stritch School of Medicine, Maywood, IL, USA. [4]Office of Research, Washington State University-Spokane, Spokane, WA, USA.
*Corresponding author. Email: vchai@luc.edu
†These authors contributed equally to this work.

STN1, also known as OBFC1 (oligonucleotide/oligosaccharide-binding fold containing 1) or AAF44, is a component of the trimeric CTC1-STN1-TEN1 (CST) complex. CST is an RPA-like single-stranded DNA (ssDNA)–binding protein complex that plays an important role in multiple genome maintenance pathways (*13*–*22*). Dysfunctional mutations in *CTC1* and *STN1* cause Coats plus syndrome, an autosomal recessive disorder characterized by bilateral exudative retinopathy, retinal telangiectasias, growth retardation, intracranial calcifications, bone abnormalities, gastrointestinal vascular ectasias, accompanied by common early-aging pathological features (*23*–*25*), and Dyskeratosis congenita, a rare genetic disease characterized by progressive bone marrow failure, skin hyperpigmentation, nail dystrophy, and oral leukoplakia (*25*, *26*). CTC1 and STN1 enhance DNA polymerase α (POLα)–primase activity (*27*), and they were initially discovered as POLα accessory factor (AAF) AAF132 and AAF44, respectively (*28*, *29*). CST binds to telomeric ssDNA and is involved in lagging strand telomere synthesis and C-strand fill-in at telomere ends (*15*, *17*, *30*–*33*). CST also restricts excessive telomerase extension of telomeres (*13*). Recent studies have revealed the crucial role of CST in maintaining genome stability when replication is perturbed. CST antagonizes unscheduled MRE11-mediated nascent strand DNA degradation at stalled replication forks, thereby protecting global genome stability under replication stress (*20*, *34*). In response to hydroxyurea treatment, CST colocalizes with RAD51 and is recruited to stalled replication forks. CST physically interacts with RAD51 and facilitates RAD51 recruitment to RPA-bound ssDNA and stalled forks (*21*, *34*, *35*). In addition, CST is recruited to DNA double-strand breaks (DSBs) by the shieldin complex (SHLD1-SHLD2-SHLD3-REV7) to promote nonhomologous end joining. Removal of CST promotes end resection, restoring homologous recombination in BRCA1-deficient cells and thus leading to Poly (ADP-ribose) polymerase (PARP) inhibitors resistance (*36*–*39*).

Recent TCGA Pan-Cancer analyses show that down-regulation of CST genes is associated with poor outcomes of patients in various cancers, identifying CTC1 and STN1 as the protective

factors in several types of cancers (*40*, *41*). Similarly, genome-wide association studies analyses have shown that STN1 variants are associated with increased risks of melanoma, leukemia, ovarian, colon, and liver cancers (*42*–*47*). These observations suggest that CTC1 or STN1 may suppress the development of cancers in humans. However, this has not been tested in vivo. In this study, we analyzed the TCGA Pan-Cancer database and found that CTC1/STN1 expression is attenuated in CRC tumors compared to normal tissues. Consistently, we observed that human colon adenocarcinoma shows reduced STN1 levels than matched normal adjacent tissue. CRCs with CTC1 or STN1 alterations show a higher tumor mutation burden and poorer survival. These observations suggest that CTC1/STN1 may play an important role in suppressing CRC tumor formation. To determine the role of STN1 deficiency in tumorigenesis in vivo, we generated an inducible *STN1* knockout mouse model. We found that STN1-deficient mice showed enhanced tumor development and higher tumor volume in the murine colon in the azoxymethane (AOM)–induced CRC mouse model. CRC tumors developed from STN1-deficient mice displayed elevated levels of c-MYC, COX-2 (cyclooxygenase 2), and β-catenin, enhanced cell proliferation, reduced apoptosis, and increased γH2AX signal. In addition, STN1 reduction slowed down replication fork speed and accumulated ssDNA in mouse embryonic fibroblast (MEF) cells. Furthermore, STN1 reduction suppressed the expression of multiple DNA glycosylase genes in the base excision repair (BER) pathway, resulting in increased oxidative damage and rendering cells sensitive to oxidation-inducing agent. We also found that STN1 expression positively correlates with the expression of various DNA glycosylase genes in human and mouse tissues. Last, we found that STN1 defective colon cancer cells showed an increased level of DNA alkylation and were sensitive to DNA alkylating agents. Together, our study identifies that mammalian STN1 suppresses colorectal tumorigenesis, likely by regulating the expression of DNA glycosylase genes and preserving the function of BER to prevent the accumulation of oxidative damage. These results highlight the importance of CST in maintaining genome stability and suppressing tumor formation. In addition, our findings uncover a previously unidentified genetic condition promoting CRC development and provide insights into the CRC tumor suppression mechanism.

RESULTS

CTC1/STN1 expression is commonly reduced in CRC, and this decrease correlates with poor prognosis

To investigate the potential role of CST in cancer, we analyzed *CTC1* and *STN1* genetic alterations (including mutations, amplifications, deep deletions, and structural variants) and expression using the TCGA database via cBioPortal (*48*). Colorectal adenocarcinoma is among the cancer types with the highest *CTC1* and *STN1* alteration frequencies (Fig. 1A and fig. S1). Mutations and deep deletions of *CTC1* and *STN1* are predominant in CRCs (Fig. 1A), whereas *TEN1* alterations more commonly show amplifications (fig. S1). In addition, the *CTC1* and *STN1* altered groups contain higher mutation counts than the unaltered group in the CRC TCGA Pan-Cancer datasets (Fig. 1B). Furthermore, both *CTC1* and *STN1* mRNA expression are down-regulated in tumor samples compared to that in normal tissues in TCGA colon and rectum cancer datasets (Fig. 1, C to F), but not *TEN1* (fig. S2A). We thus focused on analyzing *CTC1* and *STN1* in our study. We then detected STN1 protein expression using human tissue arrays containing 62 pairs of colon adenocarcinoma and matched adjacent normal tissue samples. Consistent with the TCGA mRNA down-regulation, the overall STN1 protein level was also reduced in tumors compared to normal tissue (Fig. 1G). We also tested several commercially available CTC1 antibodies but found that none were able to specifically detect CTC1 in human tissues, preventing us from measuring CTC1 protein levels in human samples. *CTC1/STN1* alteration is associated with poor overall survival (Fig. 1H). We also found that, while altered *CTC1* + *STN1* (CS) mRNA expression shows no obvious association with the overall survival in TCGA CRCs (P = 0.124), unaltered expression of *STN1* is beneficial for disease-free survival (P = 0.0186), suggesting that *STN1* expression could be a survival biomarker for CRC patients (Fig. 1I). Altered expression of *CTC1* is not significantly associated with overall or disease-free survival in TCGA CRCs (fig. S2B).

STN1-deficient mice increased CRC incidence, tumor burden, and tumor size upon AOM treatment

To investigate the potential role of STN1 in CRC initiation and development, we sought to develop an in vivo mouse model in which STN1 could be deleted. However, we could not simply generate a complete *STN1* knockout, since STN1 is required for efficient global DNA replication and cell proliferation. Mutations in STN1 lead to Coats plus syndrome in humans, an autosomal genetic disorder whose patients exhibit intrauterine growth retardation, premature aging, hypocellular bone marrow, and recurring gastrointestinal hemorrhaging (*24*). A complete *STN1* deletion is expected to cause embryonic lethality or premature death due to proliferation failure as observed in the *CTC1* knockout mice (*17*). Consistent with this notion, we failed to obtain STN1 knockout clones when using CRISPR-Cas9 to delete STN1 in human cancer cell lines. Thus, we used the Cre-*loxP* system to generate *STN1* conditional knockout (cko). The mouse *STN1* locus contains 10 exons, with the ATG start codon residing in exon 2 (Fig. 2A). When *loxP* insertion sites were initially designed, the most convenient approach to delete murine *STN1* appeared to be deleting exons 5 and 6, which would create a frameshift and generate a truncated STN1 protein. However, a long noncoding RNA (lncRNA) with unknown function is present in this region. To avoid affecting this lncRNA, we targeted the upstream regions of the STN1 gene by inserting two *loxP* sites upstream of the promoter region and downstream of the ATG start codon in exon 2 (Fig. 2A). Cre expression resulted in the deletion of the promoter sequence and the translation start site, thereby inhibiting both transcription and translation of the gene (Fig. 2A). Deleting the promoter region would also eliminate the possible complications caused by a truncated protein that could be synthesized from a downstream ATG codon. The resulting $STN1^{Flox/Flox}$ ($STN1^{F/F}$) mice were then bred with $Cre\text{-}ER^{T2}$ mice, producing $Cre\text{-}ER^{T2}$; $STN1^{F/F}$ mice, which were then confirmed by tail snip genotyping. Initial pilot experiments were performed to determine the efficiency of Cre recombination using large intestine tissues and primary MEFs isolated from $Cre\text{-}ER^{T2}$; $STN1^{F/F}$ animals. Tamoxifen treatment largely removed STN1 protein expression in MEFs, suggesting that STN1 was effectively reduced by Cre induction (Fig. 2B). However, residual STN1 protein was visible in large intestine tissues after Cre induction (fig.

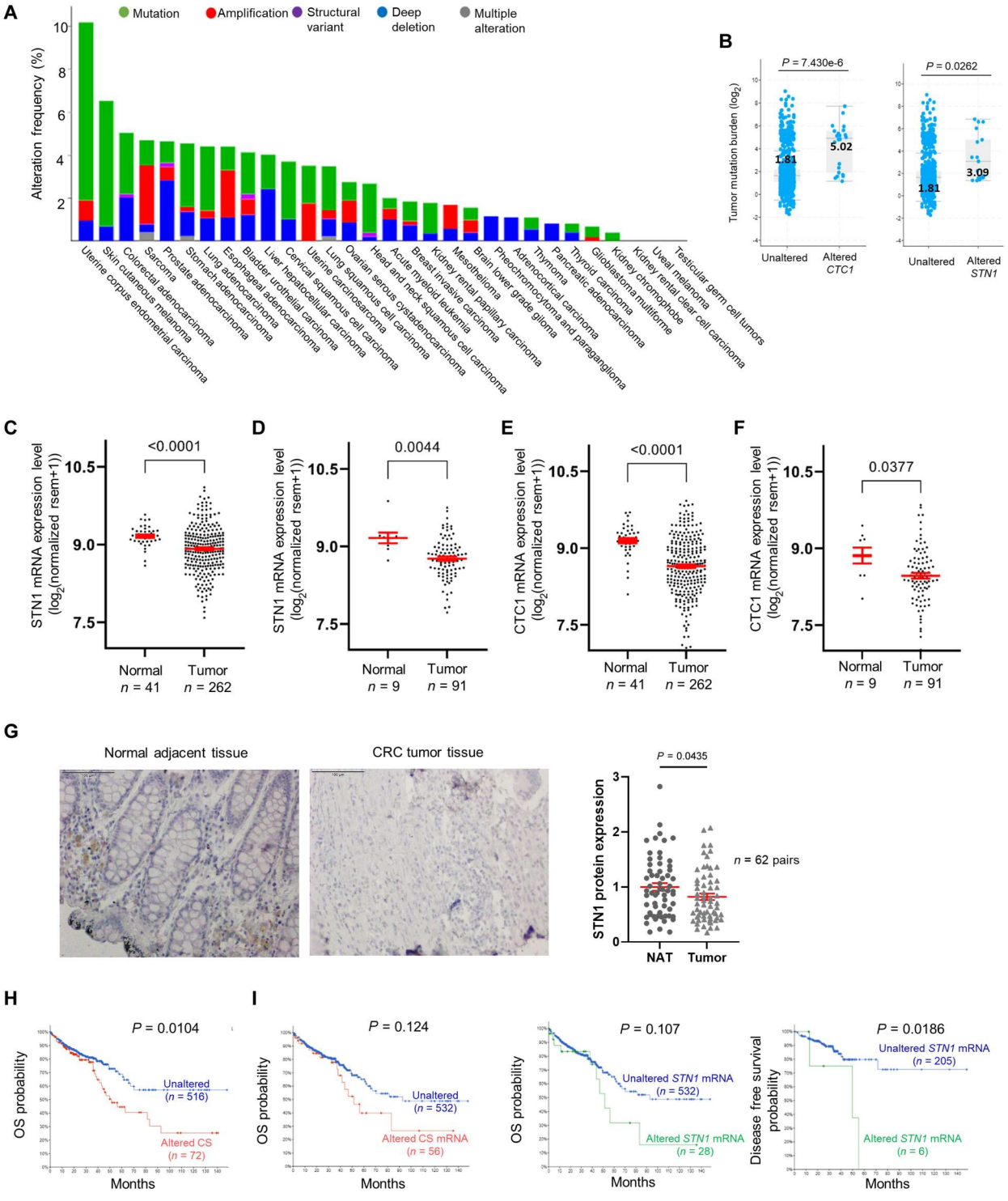

Fig. 1. Lower expression of *STN1* and *CTC1* in CRC tumor and its correlation with poor prognosis. (**A**) TCGA data analysis shows a high alteration frequency of *CTC1* and *STN1* in CRC Pan-Cancers. (**B**) TCGA Pan-Cancer analysis shows that tumor mutation burden in *STN1*- and *CTC1*-altered tumors is higher than in CRC tumors with unaltered *STN1*/*CTC1*. $P = 0.0018$. (**C** to **F**) mRNA expression levels of *STN1* (C and D) and *CTC1* (E and F) in tumors are lower than those of normal tissues in both colon (C and E) and rectum cancers (D and F) from TCGA Pan-Cancers. (**G**) Representative IHC staining of STN1 protein in human colon adenocarcinoma and matched normal adjacent tissue (NAT). Scale bars, 100 μm. STN1 protein level from a total of 62 tumor and matched normal pairs was measured and graphed. *P* values: two-tailed paired *t* tests. Error bars: SEM. (**H**) Genetic alterations of *STN1* and *CTC1*, including mutation, amplification, deep deletion, and structural variants, are correlated with poor overall survival (OS) in TCGA CRC. (**I**) Association of altered STN1 mRNA expression with poor disease-free survival in TCGA CRC, whereas there is no significant association with OS.

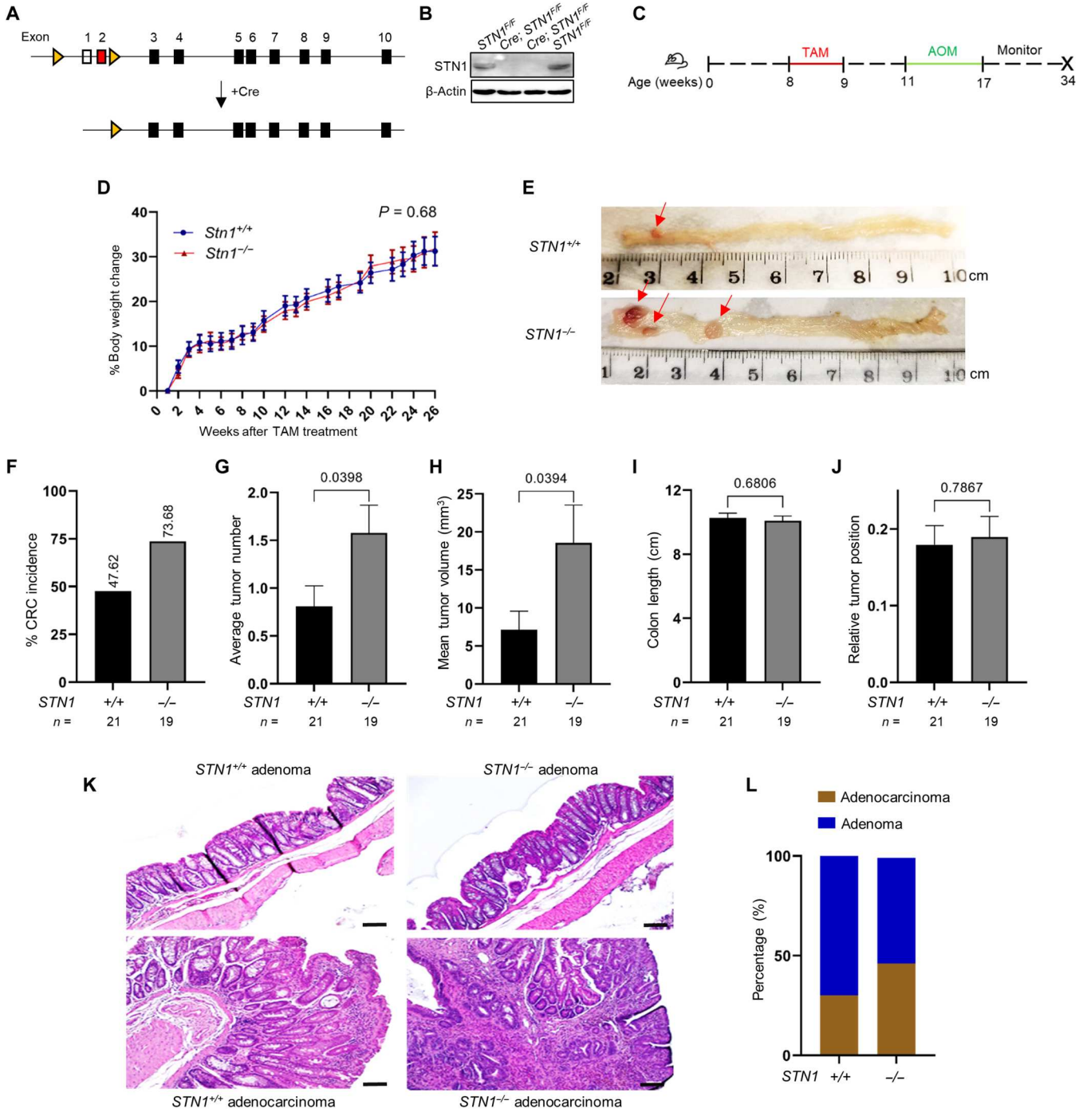

Fig. 2. STN1-deficient mice showed increased CRC development upon AOM treatment. (**A**) *STN1* allele in the mouse genome and the scheme for *STN1* cko. Open box: noncoding exon 1. Filled boxes: coding exons. The ATG start codon is located in exon 2 (red). Triangles: *loxP* sites. (**B**) Western blots showing STN1 depletion in primary MEFs after tamoxifen (TAM)-induced Cre expression. (**C**) Scheme for TAM and AOM treatment. (**D**) Percentage body weight change after TAM treatment of $STN1^{+/+}$ ($n = 21$) and $STN1^{-/-}$ ($n = 19$) mice. Data are presented as weekly % of mean body weight change ± SEM. Statistical analysis was performed using two-tailed Welch's unequal variances *t* tests. (**E**) Representative colons harvested from AOM-treated $STN1^{+/+}$ (top) and $STN1^{-/-}$ (bottom) mice at 26 weeks after TAM treatment. Red arrows point to tumors. Distal to proximal colon was oriented from left to right. (**F**) Percentage of animals developed CRC polyps in $STN1^{+/+}$ and $STN1^{-/-}$ groups. (**G**) Average CRC tumor number per mouse. (**H**) Mean tumor volume per mouse. (**I**) No significant differences in colon length between $STN1^{+/+}$ and $STN1^{-/-}$ mice. (**J**) Position of CRC polyps in $STN1^{+/+}$ and $STN1^{-/-}$ mice. Relative polyp position was calculated by the ratio of polyp distance (to anus)/colon length. (**K**) Representative hematoxylin and eosin staining of colon adenoma (top) and adenocarcinoma (bottom) from AOM-treated $STN1^{+/+}$ (left) and $STN1^{-/-}$ (right) mice. Scale bars, 100 μm. (**L**) Quantification of (K) showing that there are more high-grade tumors (adenocarcinomas) in $STN1^{-/-}$ mice compared to $STN1^{+/+}$ mice. *P* values in (G) to (J) were calculated using two-tailed *t* tests in GraphPad Prism. Error bars represent ±SEM.

S3), indicating that STN1 depletion was less robust in the heterogeneous colon tissue.

Several animal models have been developed to investigate the mechanism and preventive/therapeutic approaches for CRC in mice (*49*, *50*). Among them, the AOM-induced CRC model has been shown to be effective and is widely used (*51*–*53*). AOM is considered a colon-specific tumor initiator. AOM treatment predominantly induces tumors in the distal to the middle colon (*54*). Previously, AOM has been used to investigate the roles of DNA damage response proteins in CRC development and progression (*55*, *56*). AOM-induced murine tumors display several features of human CRC including mutations in KRAS (*57*), altered subcellular localization of β-catenin (*58*, *59*), or defective transforming growth factor–β (TGF-β) (*60*). The pathogenesis of AOM treatment in mice makes it an advantageous model to study genetic alterations in CRC development.

We treated the mice with AOM after Cre induction by tamoxifen administration and monitored CRC development after AOM treatment. Mice were sacrificed within 30 weeks following tamoxifen administration for tumor evaluation and tissue collection (Fig. 2C). In this study, both *Cre-ER^{T2}; STN1$^{+/+}$* and *STN1$^{F/F}$* (with no Cre) animals were used as controls and were referred as *STN1$^{+/+}$*, while *Cre-ER^{T2}; STN1$^{F/F}$* animals were referred as *STN1$^{-/-}$*. Physical signs including body weight, bloody diarrhea, and behavioral abnormalities were recorded, and *STN1$^{+/+}$* and *STN1$^{-/-}$* groups did not show significant differences. As expected, body weights were slightly decreased after AOM injection in both groups, but there was no significant difference between the two groups (Fig. 2D).

CRC development was evaluated at the endpoint of the experiment. Typical colon polyps were formed exclusively in the distal half of the colon in both groups (Fig. 2E). More *STN1$^{-/-}$* animals developed CRC polyps than the control group (Fig. 2F), but no gender difference in polyp formation was observed. In addition, the average tumor number per animal was notably greater in the *STN1$^{-/-}$* group (Fig. 2G). Consistent with the increased tumor burden, the average polyp size per animal was also increased in the *STN1$^{-/-}$* group (Fig. 2H). However, the average colon length and distance from tumors to the anus were similar between the two groups (Fig. 2, I and J). Furthermore, histopathological examination showed a higher percentage of adenocarcinoma in *STN1$^{-/-}$* mice compared to *STN1$^{+/+}$* mice (Fig. 2, K and L). Together, AOM-treated *STN1$^{-/-}$* mice showed an increased CRC incidence, greater tumor burden, and elevated malignancy, suggesting that mammalian STN1 plays an important role in inhibiting the development of chemically induced CRC.

Increased DNA damage, cell proliferation, and decreased apoptosis in STN1$^{-/-}$ mouse colon

AOM is a genotoxic agent that induces DNA methylation and oxidative damage in the colon. Given the vital role of STN1 in protecting genome integrity in human cells (*34*, *35*, *61*), STN1 may protect genome stability against AOM-induced DNA damage in colon tissues. To assess this possibility, sections of the colon from *STN1$^{-/-}$* and *STN1$^{+/+}$* mice were immunostained with anti-γH2AX to detect DNA damage. We observed stronger γH2AX immunohistochemical (IHC) staining signals in *STN1$^{-/-}$* mice relative to *STN1$^{+/+}$* mice (Fig. 3A).

Using the cell proliferation marker protein Ki67, we detected higher Ki67 expression in the colon tissue from the *STN1$^{-/-}$* group than in the *STN1$^{+/+}$* group (Fig. 3B). In addition, terminal deoxynucleotidyl transferase–mediated deoxyuridine triphosphate nick end labeling (TUNEL) analysis detected a reduction in apoptosis in *STN1$^{-/-}$* tumors (Fig. 3C). These results indicate that tumors developed in *STN1$^{-/-}$* mice are highly proliferative, and STN1 likely maintains the balance between proliferation and apoptosis in the colon in AOM-treated mice.

STN1 deficiency increased tumor markers in AOM-treated mouse colon

The occurrence of AOM-induced CRC is a complex process, including the activation of multiple signaling pathways relating to DNA damage and inflammation. The administration of AOM causes APC mutations, activating its downstream pathways including the nuclear factor κB (NF-κB) and WNT/β-catenin signaling pathways (*62*, *63*). In addition, overexpression of COX-2 is a frequent event in CRC, and it has been shown that p53-mediated induction of COX-2 prevents apoptosis after DNA damage (*64*). Our IHC analysis showed enhanced staining of COX-2 and β-catenin in *STN1$^{-/-}$* colon tissues (Fig. 3, D and E). Consistently, c-MYC, which is downstream of the WNT signaling pathway, also showed a higher expression in the *STN1$^{-/-}$* colon tissue (Fig. 3F). All together, these results suggest that STN1 deficiency enhances the survival of cancer cells and promotes hyperproliferation by increasing COX-2 expression and activating the WNT/β-catenin signaling.

STN1 deficiency elevated genome instability in human colon cancer cells and MEFs

An unstable genome is a tumor-initiating factor driving tumor development (*8*, *65*, *66*), although it is still debatable whether genome instability is the cause of cancer or the consequence of tumor cell growth. To elucidate the mechanism underlying the increased CRC formation in STN1-deficient mice, we tested whether STN1 deficiency affected genome stability using both the human colon cancer cell line and MEFs isolated from *STN1$^{-/-}$* mice. Historically, AOM treatment was primarily conducted in vivo and limited information is available on AOM treatment in cells. Thus, we first tested AOM treatment condition in the human colon cancer cell line HCT116. HCT116 cells were treated with a range of AOM concentrations from 0.05 to 5 μg/ml for 30 min and then grown overnight for cell survival measurements (fig. S4). A sublethal concentration of AOM (1.25 μg/ml) was chosen for the following in vitro experiments.

Using comet assays, we observed that depletion of STN1 in both HCT116 and MEFs led to an increased percentage of tail DNA (Fig. 4A), suggesting an increase in intrinsic DNA damage upon STN1 depletion. As expected, AOM treatment increased the percentage of tail DNA in both the control and STN1-depleted HCT116 cells and MEFs (Fig. 4A). Likewise, we observed an increase in γH2AX staining in *STN1$^{-/-}$* MEFs with or without AOM treatment (Fig. 4B). These results were consistent with previous reports that STN1 deficiency induces DNA damage in various human cell lines including HeLa, U2OS, and HCT116 (*30*, *67*, *68*). Since studies have found the crucial function of STN1 and the CST complex in telomere maintenance (*15*, *17*, *30*–*33*), we measured telomere dysfunction–induced DNA damage (TIFs) using γH2AX staining combined with telomere fluorescence in situ hybridization (FISH). While we observed an increase in telomere DNA damage, the number of TIFs was low (less than five TIFs per cell) (fig. S5).

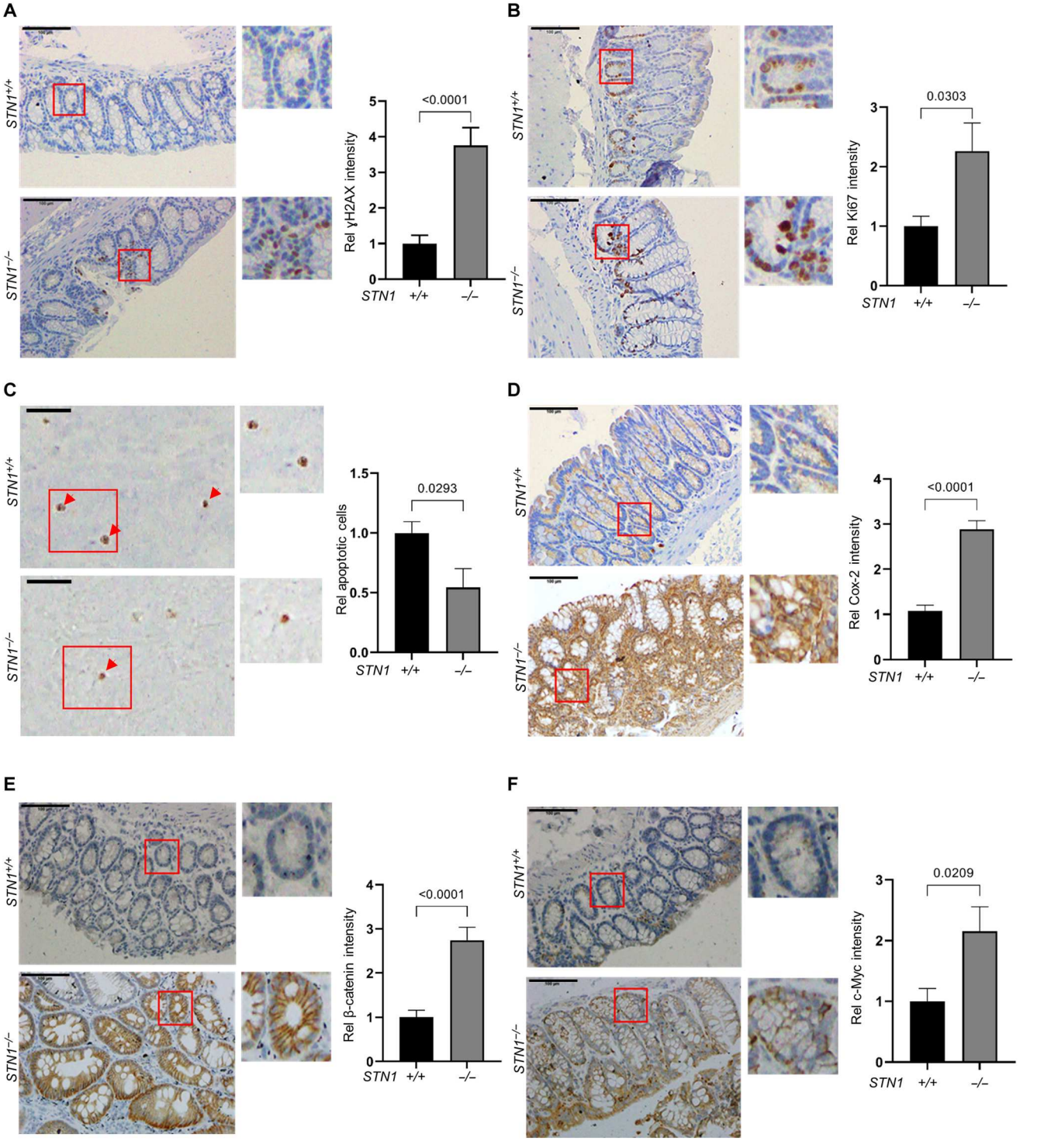

Fig. 3. Effects of STN1 deficiency on CRC tumor markers, cell proliferation, apoptosis, and DNA damage in mouse colon tissue. (**A**) Representative IHC staining of γH2AX showed a higher DNA damage level in *STN1*$^{-/-}$ mice. Boxed areas are magnified to show staining details. (**B**) IHC staining with Ki67 showed a higher cell proliferation level in *STN1*$^{-/-}$ mice. (**C**) TUNEL assay showed that *STN1*$^{-/-}$ mouse colon tumor displayed reduced cell apoptosis. Red arrows point to apoptotic cells. Data are shown as the relative average number of apoptotic cells per image. Scale bars, 20 μm. (**D** to **F**) IHC staining showed higher expression of tumor markers β-catenin (D), Cox-2 (E), and c-Myc (F) in *STN1*$^{-/-}$ mice. For all IHC staining and TUNEL assays, the paraffin-embedded distal colon tissues from four pairs of mice [*STN1*$^{+/+}$ ($n = 4$) versus *STN1*$^{-/-}$ ($n = 4$)] were processed for staining. In all IHC images, scale bars are 100 μm. IHC signals were quantified using ImageJ. At least 5000 cells were measured in each group. All signals were normalized to the *STN1*$^{+/+}$ group, and relative intensities were graphed. Statistical analysis: two-tailed *t* tests. Error bars: SEM.

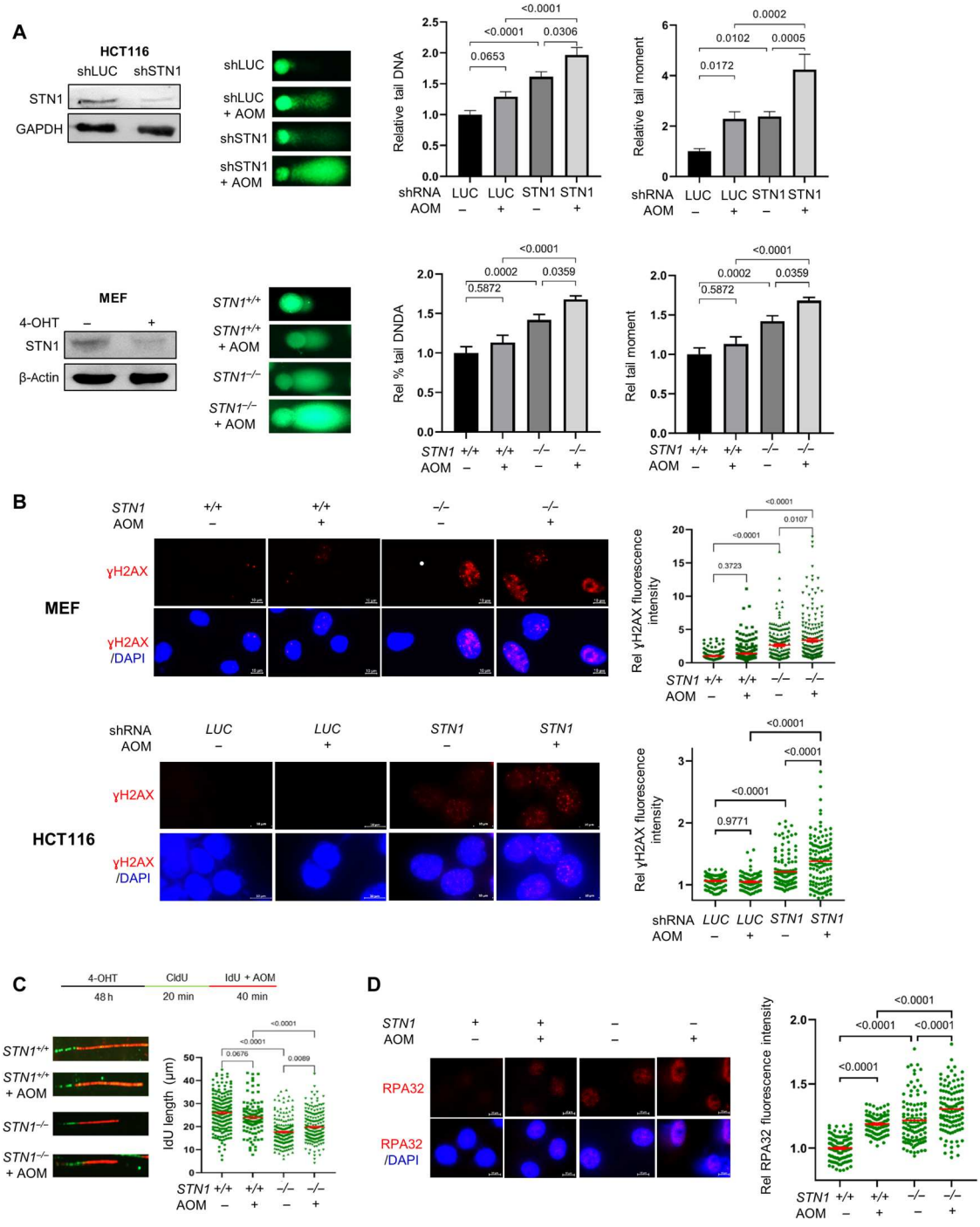

Fig. 4. STN1 deficiency induced genome instability and reduced replication fork speed in human and mouse cells. (**A**) Representative comet images from HCT116 cells and MEFs. Western blotting showed effective depletion of STN1 in HCT116 cells after knockdown and in *CreER*^{T2};*STN1*$^{F/F}$ MEFs after 48 hours of 4-OHT treatment, respectively. Cells were then treated with or without 1.25 μM AOM for 30 min. Alkaline comet assay was performed to detect damaged DNA. Relative percentage of tail DNA and tail moment per nucleus was presented. Two independent experiments were performed, and the result from one experiment is shown. In each experiment, at least 100 cells per sample were selected from random fields for comet analysis. (**B**) Representative γH2AX IF images in immortalized MEF cells and HCT116 after STN1 depletion. Relative intensity of γH2AX fluorescence per nucleus was measured using ImageJ. Two independent experiments were performed, and the result from one experiment is shown. Scale bars, 10 μm. In each experiment, >100 cells were analyzed per sample. (**C**) Scheme of DNA fiber assay and representative DNA fiber images. Following *STN1* depletion in immortalized MEF cells by 48 hours of 4-OHT treatment, cells were sequentially labeled with CldU and IdU ± AOM. Two independent experiments were performed, and the result from one experiment is shown. In each experiment, >200 fibers were measured per sample. (**D**) Representative images from RPA32 immunostaining in immortalized MEF cells. Following 48 hours of 4-OHT treatment to induce Cre expression, MEF cells were treated ± AOM for 30 min, fixed on slides, and then immunostained with RPA32. In each experiment, >100 cells were analyzed per sample. Relative intensity of RPA32 fluorescence per nucleus was measured using ImageJ. Scale bars, 10 μm. One-way analysis of variance (ANOVA) tests were performed to calculate *P* values in all figures. Error bar: ±SEM.

Notably, the vast majority of γH2AX foci were formed outside telomeres (fig. S5), consistent with previous observations that CST deficiency causes genomic damage (*20*, *35*, *69*). Our observations were also in agreement with previous reports that the human CST complex does not present a telomere capping function (*30*, *68*, *70*). We think that the global genome instability plays an important role in CRC tumorigenesis, and telomere instability may further destabilize the genome and contributes to CRC tumorigenesis.

Next, we performed DNA fiber assays using MEFs with or without AOM treatment. Following STN1 deletion by 48 hours of Cre induction, MEF cells were sequentially pulse-labeled with thymidine analogs chlorodeoxyuridine (CldU) for 20 min and iododeoxyuridine (IdU) for 40 min ± AOM to induce DNA damage (Fig. 4C). IdU lengths in *STN1*$^{-/-}$ MEFs were substantially shorter than those in *STN1*$^{+/+}$ MEFs regardless of AOM treatment, indicating that STN1 deficiency slowed down replication speed (Fig. 4C).

In human cells, CST depletion leads to accumulation of ssDNA in the telomeric region (*13*, *17*, *30*). Next, we examined the effect of STN1 deficiency on ssDNA production in murine cells by measuring RPA staining. STN1 reduction markedly increased the amount of ssDNA in MEFs (Fig. 4D), suggesting that STN1 loss leads to aberrant ssDNA accumulation. Together with our observation that the colon tissues from *STN1*$^{-/-}$ mice displayed more robust γH2AX signals (Fig. 3A), these results suggest that STN1 deficiency led to an intrinsic increase of DNA damage, and AOM treatment further elevated the damage.

Mutational signatures associated with STN1-deficient CRC tumors

The elevated genome instability observed in *STN1*$^{-/-}$ colon tissue prompted us to hypothesize that STN1 deficiency led to genomic changes that favored tumor development. To test this, we analyzed somatic variants in CRC tumors developed in mice. Whole-exome sequencing (WES) was performed on matched pairs of tumor-normal tissue samples isolated from three *STN1*$^{+/+}$ and three *STN1*$^{-/-}$ pairs. An average coverage depth of 256× (minimum 151×) was reached. For each animal, we measured and normalized somatic mutations in DNA isolated from tumor tissues to somatic mutations present in adjacent normal tissues to remove the influence caused by genetic variations among individual animals. No difference was observed in total mutation numbers or any kind of high-effect genetic mutations such as frameshift mutations, missense variants, or stop/gain mutations (Fig. 5A and fig. S4A). We also checked the mutation numbers of tumor markers for CRC to determine whether *STN1*$^{-/-}$ would affect CRC marker genes. We observed higher mutation numbers of *Nras*, *Braf*, and *Ctnnb1* and lower mutation numbers of *Brca2*, *Smad4*, and *c-Myc* in *STN1*$^{-/-}$ tumors compared to the *STN1*$^{+/+}$ group (fig. S4B). However, because of the low number of samples, the differences were not statistically significant between the two groups. Future studies with more samples are needed for a conclusive result.

Somatic variants in cancer have been shown to target nucleotides in specific sequence contexts, and they are referred to as mutational signatures (*71*). Mutational signatures can be used to infer the underlying cause of the mutations and have recently been used as a powerful tool to identify the specific mutagenic events (such as exposure to a chemical or environmental toxin, or a particular type of DNA damage) that led to the cancer-causing mutations. They can provide important insights into the etiology of cancer development. We then examined whether the mutational signatures from our mice were associated with mutational signature profiles in human cancer (*72*). We performed mutational signature extraction from six somatic mutation profiles from WES samples using the COSMIC signature catalog. In total, six single-base substitution (SBS), four double-base substitution (DBS), and two INDEL (ID) profiles were extracted from COSMIC Signature Profiler (https://cancer.sanger.ac.uk/signatures/). Extracted signatures from the COSMIC catalog of both *STN1*$^{-/-}$ and *STN1*$^{+/+}$ mice showed a strong association with the SBS5 mutational signature, in which colorectal adenocarcinoma profiles from the TCGA database expressed the topmost mutation burden (Fig. 5B and fig. S4C). SBS5 is a clock-like signature with a "featureless" mutation spectrum appearing in most types of cancer samples, and the number of mutations seems to correlate with the age of the individual (*71*). Rates of acquisition of SBS5 mutations over time differ between different cancer types and different normal cell types. While the proposed etiology of SBS5 is still under investigation, one proposed etiology for this signature is high levels of oxidative stress (*73*), although this association still needs experimental validation. In addition, *STN1*$^{-/-}$ mice also showed higher mutational signature SBS25 (Fig. 5B) and reduced mutational signatures SBS8 and SBS37 (Fig. 5B), all of which have undefined etiology and unknown contributions to CRC development. Because of the lack of experimental validation of many SBS signatures, future genomic investigations are needed to determine the significance and implication of these mutational signatures in cancer etiology.

STN1 deficiency suppresses the expression of DNA glycosylases, leading to elevated oxidative DNA damage

To further analyze somatic mutations caused by STN1 reduction, we then used our WES data to investigate the effect of STN1 deficiency on mutation rates within genes in the DNA repair pathways (GO:0006281). After overlapping high-confidence somatic mutations within genes that function in DNA repair, we found that *STN1*$^{-/-}$ mice displayed higher mutation numbers in *FANCF*, *FANCG*, and *FANCI* in the Fanconi anemia (FA) pathway; *MSH3* in the MMR pathway; *INO80*, *MRE11*, and *RAD52* in homologous recombination repair (HR); and multiple genes in the BER pathway including *OGG1*, *SMUG1*, *NEIL2*, and *POL*B (table S1). A complete list of DNA repair genes showing increased variations is provided in table S1.

The BER pathway is the major pathway for repairing oxidative damage, and defective BER is expected to cause an increase in oxidative damage. Numerous studies have found the association between oxidative stress with colorectal tumorigenesis (*74*–*76*). In addition, BER has been shown to protect against AOM-induced colon carcinogenesis (*77*). Given that multiple BER genes, in particular DNA glycosylase genes *OGG1*, *SMUG1*, and *NEIL2*, showed higher mutation numbers, we analyzed TCGA Pan-Cancer CRC datasets and found a higher frequency of BER gene alterations in CRC tumors containing *STN1* alterations (Fig. 6A). Using the TCGA Pan-Cancer and Genotype-Tissue Expression (GTEx) datasets (*78*), we also found that *STN1* mRNA expression level positively correlated with *OGG1*, *SMUG1*, *NEIL2*, *MBD4*, and *MPG* gene expression in human colon tumor tissues (Fig. 6B). Likewise, positive correlations between m*STN1* mRNA expression and m*OGG1*, m*SMUG1*, m*NEIL2*, m*MBD4*, and m*MPG* gene expression were

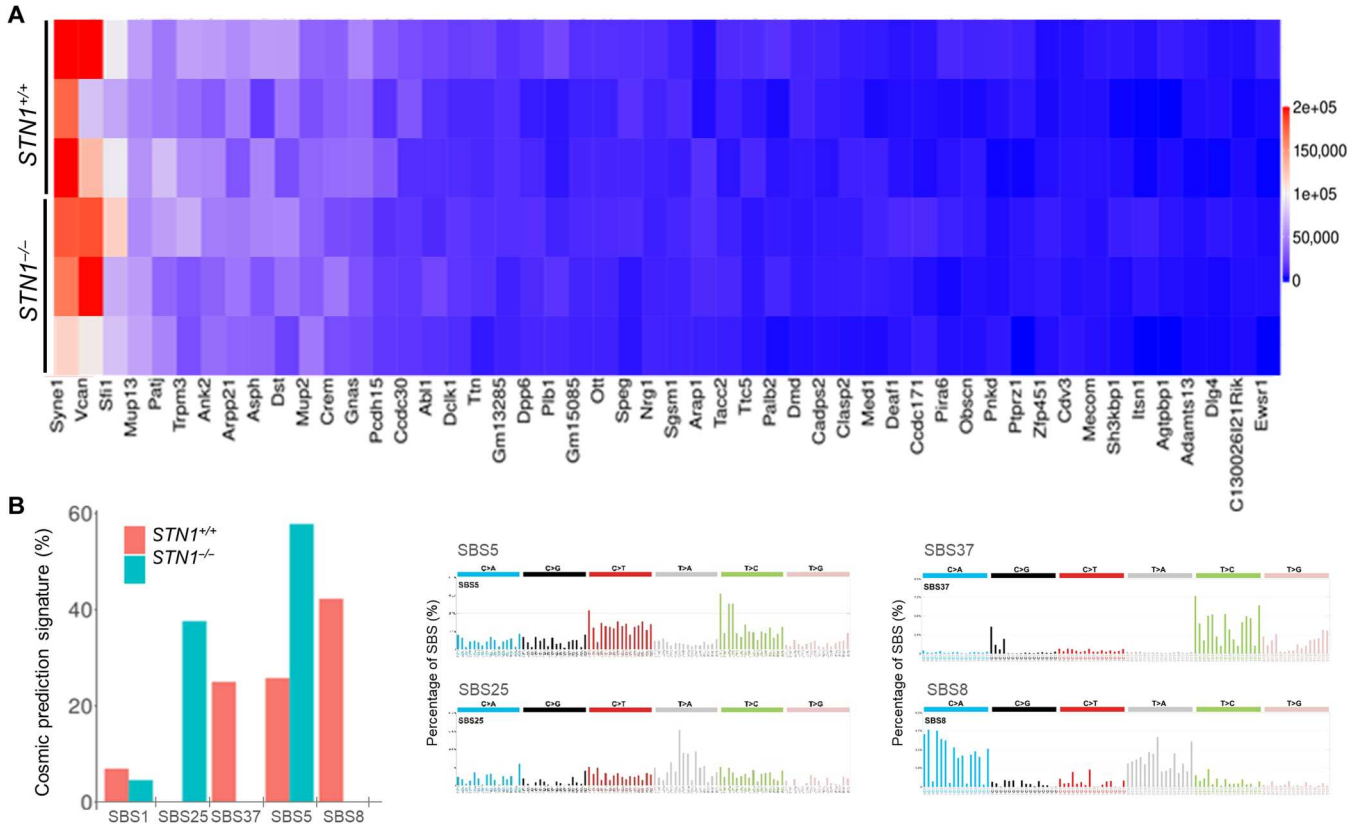

Fig. 5. WES profiles from colon tumors developed in *STN1*$^{+/+}$ (*n* = 3) and *STN1*$^{-/-}$ (*n* = 3) mice. (**A**) Heatmap of top 50 genes with the highest variant number. Similar enrichments among *STN1*$^{+/+}$ and *STN1*$^{-/-}$ mice were observed. (**B**) CRC tumors developed in *STN1*$^{-/-}$ mice show an enrichment of SBS5 and SBS25 mutational signatures and reduction of SBS8 and SBS37 signatures.

also observed in the mouse gene expression dataset (*79*, *80*) (Fig. 6B). Next, we analyzed the effect of STN1 deficiency on the expression of these genes in cells. As shown in Fig. 6C, STN1 depletion reduced the mRNA expression of *SMUG1* and *NEIL2* in MEFs, whereas mRNA level changes of *OGG1*, *MBD4*, and *MPG* were not significant (Fig. 6C). Since mRNA levels are often poorly correlated with protein expression, we then measured protein levels. We found that mSMUG1 and mNEIL2 were markedly decreased in MEFs upon STN1 reduction. We were unable to check mOGG1 expression in MEFs due to the failure of the OGG1 antibody detecting murine OGG1. To determine whether STN1 deficiency induced a similar reduction of glycosylase expression in human colon cells, we depleted STN1 using RNA interference (RNAi) in HCT116 and found that the protein expression of human OGG1, SMUG1, and NEIL2 was also markedly reduced (Fig. 6D), while POLβ expression was slighted increased (fig. S7A). Similarly, depleting CTC1 in HCT116 led to reduced OGG1, SMUG1, and NEIL2 expression (Fig. 6D).

To determine whether STN1 deficiency altered the expression of other DNA repair proteins in human colon cells, we depleted STN1 in HCT116 and measured protein levels using Western blotting. No obvious change was observed in the protein expression of FANCG, FANCI, INO80, RAD52, MRE11, and MSH3 that showed high number of mutations in our WES analysis (fig. S7A). In addition, STN1-deficient cells did not display sensitivity to mitomycin C (MMC) or cisplatin, both of which induce intra- and interstrand cross-links that can be repaired by the FA and HR pathways (fig. S7B). These results suggest that these two pathways were unlikely affected by STN1 deficiency, or perhaps other repair pathways might have compensated for the defects. However, our results cannot entirely discount the possibility that MMR may be affected by STN1 deficiency, as it has been shown that MMR can also participate in repairing oxidative damage (*81*).

STN1 deficiency leads to elevated oxidative DNA damage and sensitivity to oxidative damaging agent

DNA glycosylases OGG1, SMUG1, and NEIL2 are mainly involved in recognizing and excising oxidative DNA lesions. Defects in these genes are expected to increase oxidative damage. We thus used a modified comet assay known as the Fpg comet assay to detect unrepaired oxidative DNA lesions in single cells using Fpg in conjunction with the comet assay (Fig. 6E). Fpg (formamidopyrimidine [fapy]-DNA glycosylase, also known as 8-oxoguanine DNA glycosylase) is a bifunctional DNA glycosylase with both N-glycosylase and AP lyase activities. Its N-glycosylase activity converts damaged purines to abasic sites (AP sites). Its AP lyase activity then cleaves the AP site, creating an ssDNA break that can be detected by an alkaline comet assay (Fig. 6E) (*82*, *83*). MEF cells were treated with 4-hydroxytamoxifen (4-OHT) to induce STN1 deletion and then treated with or without AOM. Cells were then harvested, immobilized in a layer of low melting point agarose on the comet slide, gently lysed, and then treated with exogenous Fpg protein to

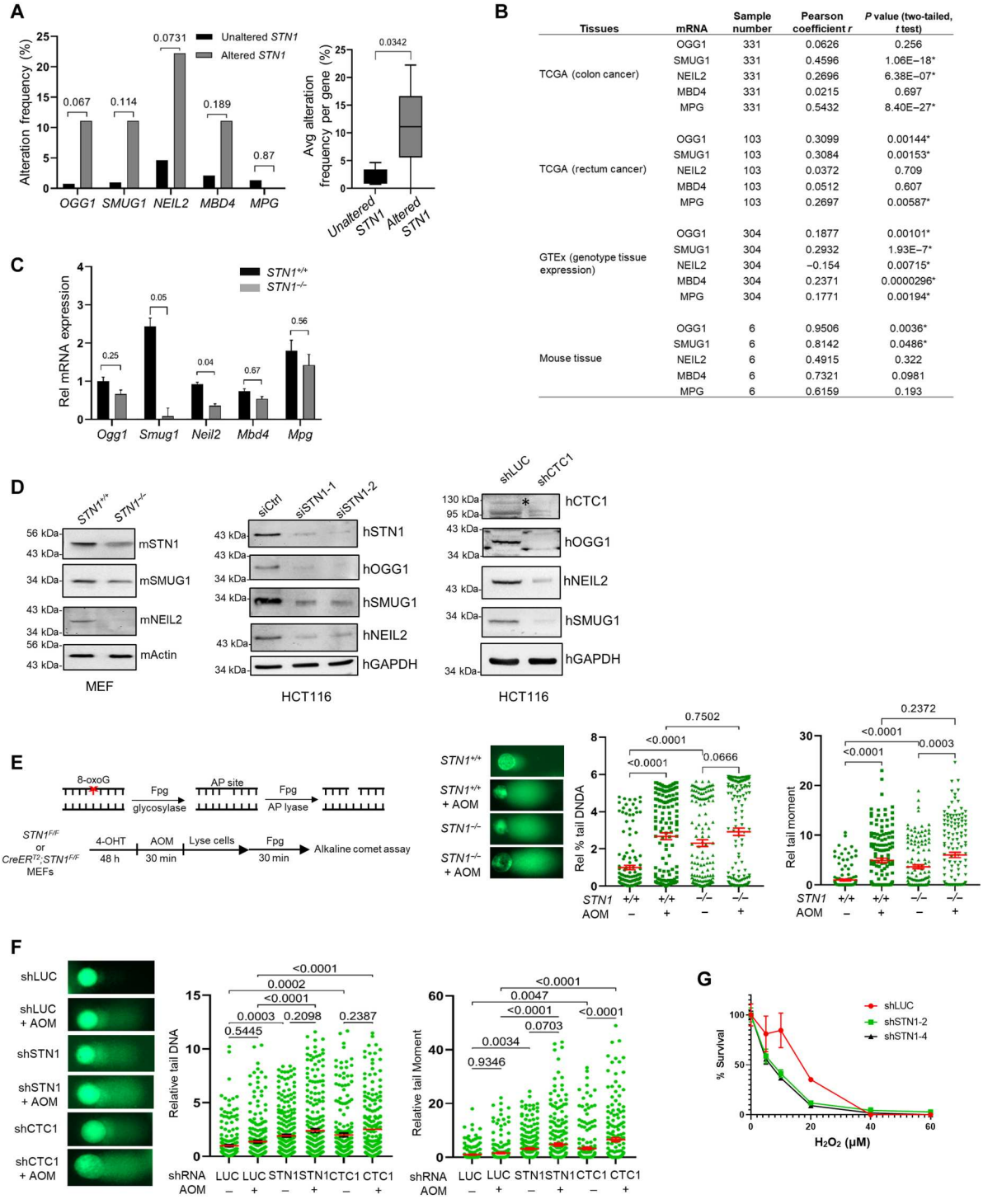

B

Tissues	mRNA	Sample number	Pearson coefficient *r*	*P* value (two-tailed, *t* test)
TCGA (colon cancer)	OGG1	331	0.0626	0.256
	SMUG1	331	0.4596	1.06E−18*
	NEIL2	331	0.2696	6.38E−07*
	MBD4	331	0.0215	0.697
	MPG	331	0.5432	8.40E−27*
TCGA (rectum cancer)	OGG1	103	0.3099	0.00144*
	SMUG1	103	0.3084	0.00153*
	NEIL2	103	0.0372	0.709
	MBD4	103	0.0512	0.607
	MPG	103	0.2697	0.00587*
GTEx (genotype tissue expression)	OGG1	304	0.1877	0.00101*
	SMUG1	304	0.2932	1.93E−7*
	NEIL2	304	−0.154	0.00715*
	MBD4	304	0.2371	0.0000296*
	MPG	304	0.1771	0.00194*
Mouse tissue	OGG1	6	0.9506	0.0036*
	SMUG1	6	0.8142	0.0486*
	NEIL2	6	0.4915	0.322
	MBD4	6	0.7321	0.0981
	MPG	6	0.6159	0.193

Fig. 6. STN1 deficiency suppressed the expression of DNA glycosylases, leading to accumulation of oxidative DNA damage. (**A**) Alteration frequency of each DNA glycosylase gene (left) and all five glycosylase genes as a group (right) from TCGA CRC Pan-Cancer data analysis in unaltered and altered *STN1* samples. *P* values: two-tailed *t* tests. (**B**) Expression correlation of STN1 and DNA glycosylase mRNA in human and mouse tissues. * indicates significant difference. (**C**) qPCR of various DNA glycosylase gene mRNA expression in MEF cells. *P* values: two-tailed *t* tests. Error bars: ±SEM. (**D**) Western blot detecting the expression of various DNA glycosylases in MEFs and HCT116 cells depleted of STN1 or CTC1. Mouse β-actin and human GAPDH were loading controls in MEFs and HCT116, respectively. For HCT116 cells treated with siRNA, cells were collected 48 hours after siRNA transfection for Western blot analysis. * indicates the correct CTC1 band. (**E**) Alkaline comet assay plus Fpg treatment using MEF cells. STN1 was depleted from MEF cells with 48-hour 4-OHT treatment. Cells were then treated ± AOM for 30 min, and alkaline comet assay plus Fpg treatment were performed. *P* values: one-way ANOVA. Error bars: ±SEM. (**F**) Alkaline comet assay plus Fpg treatment using HCT116 cells after STN1 or CTC1 knockdown. HCT116 cells expressing shSTN1 or shCTC1 were treated ± AOM for 30 min, and alkaline comet assay plus Fpg treatment were performed. *P* values: one-way ANOVA. Error bars: ±SEM. (**G**) Colony formation assay of HCT116 cells with STN1 knockdown after H_2O_2 treatment. Error bars: ± SD.

remove 8-oxoguanine. The slides were then immersed in an alkaline solution to unwind the DNA strands, followed by gel electrophoresis. The denatured, cleaved DNA fragments migrate out of the cell under the influence of an electric field, whereas undamaged supercoiled DNA remains within the confines of the nuclear cell membrane. Evaluation of the DNA "comet" tail shape and migration pattern after staining with a fluorescent DNA intercalating dye allows for assessment of the extent of DNA damage. We found that STN1 deficiency in MEFs led to increased DNA breaks after Fpg treatment, indicative of elevated oxidative DNA damage (Fig. 6E). Knocking down STN1 or CTC1 in HCT116 cells produced a similar increase of oxidative damage (Fig. 6F).

Defective BER is expected to cause sensitivity to oxidative damaging agents. We found that HCT116 cells with STN1 suppression showed increased sensitivity to hydrogen peroxide (H_2O_2) (Fig. 6G). Together, these results further support that the repair of oxidative damage is defective in STN1-deficient cells.

STN1-deficient cells accumulate DNA alkylation and are sensitive to DNA methylating agents

BER is also the primary pathway for repairing alkylating lesions. Among the 11 DNA glycosylases, two glycosylases are responsible for repairing alkylating DNA lesions. MPG (also known as MDG or AAG) recognizes and cleaves alkylated bases, and TDG can remove methylated cytosine. While we did not observe protein expression changes in MPG (fig. S7A) or increased mutations in TDG (table S1), it has been shown that NEIL2 is important for promoting TDG's activity in DNA demethylation (*84*). In addition, it has been shown that increased oxidative DNA damage can cause dynamic changes in DNA methylation (*85*). Thus, we measured the accumulation of alkylating DNA damage in STN1-deficient cells using a modified AAG-APE1 assay (*86*) combined with the comet assay. Similar to the Fpg comet assay above, MEF cells were embedded in low melting point agarose on the comet slide, gently lysed, and then treated with exogenous AAG glycosylase to cleave and remove the alkylated bases, followed by APE1 endonuclease treatment to cleave the DNA phosphodiester backbone, generating strand breaks that can be detected by the neutral comet assay (Fig. 7A). Our result showed that upon STN1 loss, there is an increase in alkylating DNA damage in the cells (Fig. 7A).

While persistent DNA damage is a major force driving carcinogenesis, it can also be targeted for therapeutic purposes. DNA alkylation chemotherapy is one of the most widely used systemic therapies for cancer, yet the therapeutic effectiveness is greatly limited because of highly variable clinical responses and toxicities among individuals. Specific targeting of BER defective cancer cells can overcome these limitations because these cells are more sensitive to alkylating agents due to the lack of efficient repair. We thus treated HCT116 cells depleted of STN1 with the DNA alkylating agent methyl methanesulfonate (MMS) and a chemotherapeutic alkylating agent temozolomide (TMZ). Down-regulation of STN1 with two different short hairpin RNA (shRNA) sequences resulted in MMS sensitivity (Fig. 7B), consistent with the previous report (*61*). STN1-deficient cells also showed sensitivity to TMZ, although milder than MMS (Fig. 7B).

DISCUSSION

With the rising cases of sporadic CRC in young adults, there is an urgent need to identify new risk factors for CRC (*2*). Despite the fact that one-third of CRC patients have a family history of the disease, specific genetic conditions of ~80% of them have not been identified (*6*). The CST complex has emerged as an important player in multiple genomic maintenance pathways including protecting replication fork stability under replication stress, DSB repair, and protecting telomere integrity (*22*). However, its role in carcinogenesis has not been investigated. In this study, we identify that STN1, a component of the CST complex, suppresses AOM-induced CRC development. Our results show that the overall STN1 level is lower in CRC tumor samples than in normal adjacent tissue (Fig. 1G). We found that STN1 reduction in young adult mice leads to increased CRC tumor incidence, tumor size, and tumor burden, accompanied by elevated DNA damage and retarded DNA replication progression. These results are in line with the observations that STN1 and CTC1 are often down-regulated in human CRCs (Fig. 1, C to G) and CTC1/STN1 alteration is associated with poor overall survival (Fig. 1H). Furthermore, higher expression of STN1 is beneficial for disease-specific survival in CRCs (Fig. 1I). We uncovered that both STN1 and CTC1 are required for robust expression of a group of BER DNA repair genes. STN1 or CTC1 reduction attenuates the expression of *OGG1*, *SMUG1*, and *NEIL2* glycosylases (Fig. 6D), which are responsible for recognizing and excising oxidized DNA lesions to initiate the BER process that restores the regular DNA structure with high accuracy. Consequently, STN1 down-regulation led to increased oxidative DNA damage in cells (Fig. 6, E and F). Oxidative damage plays an important role in colorectal carcinogenesis, as demonstrated by hereditary syndromes (MUTYH-associated polyposis and NTHL1-associated tumor syndrome) with high-penetrant risk factors for adenomatous polyposis and CRC, where germline mutations cause loss of function in the glycosylase MUTYH or NTHL1 (*76*). While our results cannot completely rule out that other repair pathways are impaired by STN1 deficiency, we propose that functional STN1 (and perhaps the CST complex) is required for proper expression of a subset of BER genes. STN1 deficiency attenuates the expression of DNA glycosylases and causes accumulation of oxidative DNA damage and DNA alkylation due to defective BER, leading to genome instability that promotes colorectal tumorigenesis (model in Fig. 7C). Our study shows that STN1 can influence proliferation, apoptosis, and DNA repair in tumorigenesis in vivo and will help in uncovering previously unknown genetic conditions beyond the currently known germline mutations.

Unlike CTC1 and STN1, TEN1 mutations have not been reported in Coats plus patients. In addition, TEN1 is often amplified in various cancers as shown by TCGA analysis (fig. S1), and there appears to be no association of TEN1 expression with CRC (fig. S2A). The specific reason underlying the difference between TEN1 and CTC1/STN1 is still unknown, and these observations suggest that TEN1 likely has a function separate from CTC1 and STN1. To date, studies on mammalian CST have been primarily focused on analyzing CTC1 and, to a lesser degree, STN1. Further investigations are needed to understand the biological functions of TEN1 and its possible role in CRC pathogenesis if there is any.

Although the $CreER^{T2}$;$Stn1^{F/F}$ mice used in this study showed partial STN1 deletion after tamoxifen administration, it generated

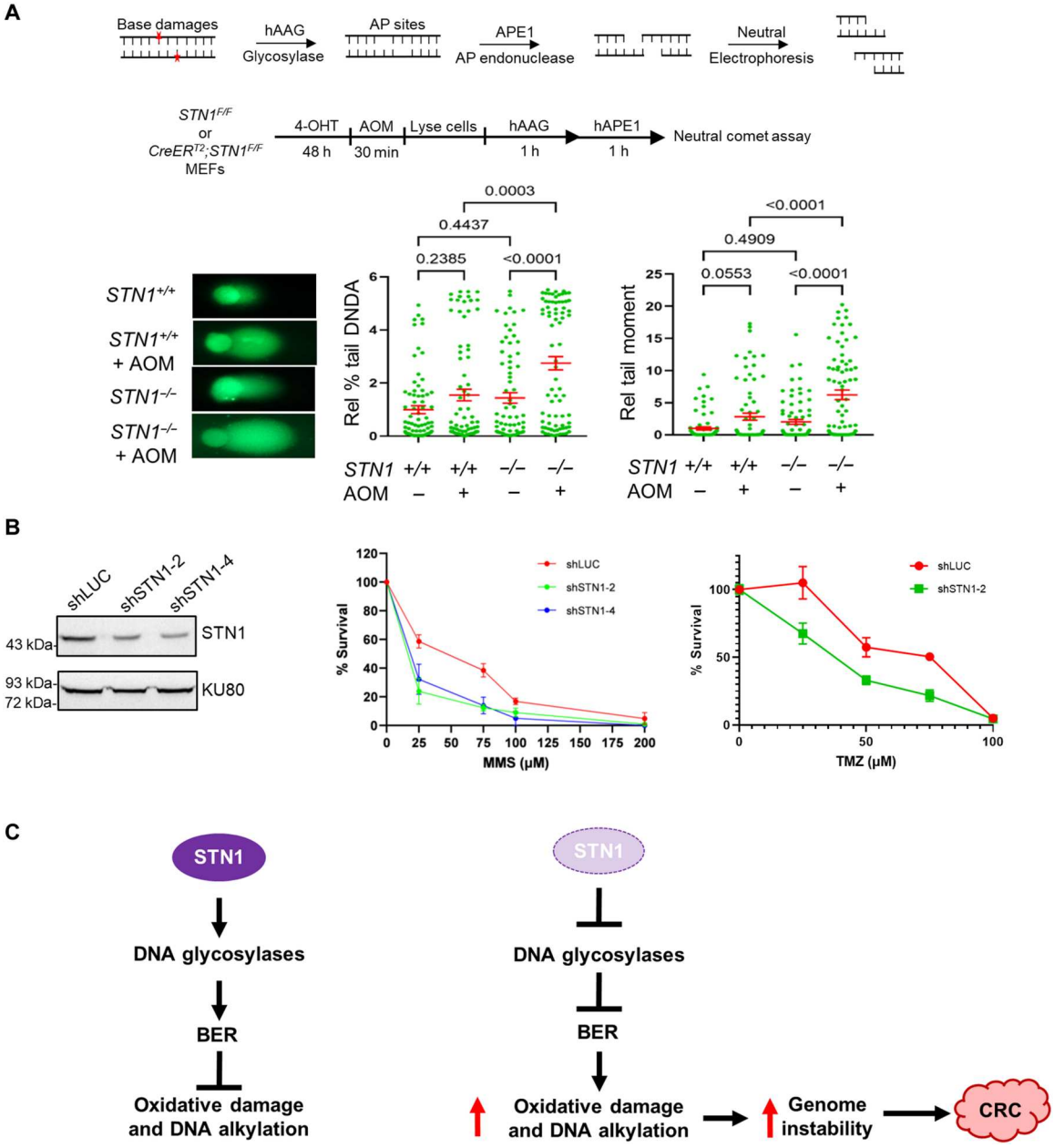

Fig. 7. STN1 deficiency renders colon cancer cells sensitive to DNA alkylating agents. (**A**) AAG-APE1 comet assay. STN1 was depleted from MEF cells with 48-hour 4-OHT treatment. Cells were then treated ± AOM for 30 min, and the AAG-APE1 comet assay was performed. *P* values: one-way ANOVA. Error bars: ±SEM. (**B**) Colony formation assays of HCT116 cells with STN1 knockdown after MMS or TMZ treatment. Western blot shows the STN1 knockdown level. Error bars: SD. (**C**) Model: STN1 plays a tumor suppression role by ensuring the robust expression of DNA glycosylase genes and preserving the BER pathway, thereby preventing genome instability and suppressing CRC tumorigenesis.

the STN1 reduction model that more closely resembled the decreased STN1 expression observed in human CRC samples (Fig. 1E). Thus, we consider that this mouse model is suitable for studying the role of STN1 deficiency in promoting tumorigenesis. Moreover, if STN1 had been efficiently deleted, it might have caused proliferation failure resembling CTC1 deletion (*17*) that prevented tumor formation. None of the Coats plus patients developed cancer, likely because they suffered from serious chronic gastrointestinal bleeding and did not survive long enough for cancer development.

The following possibilities may explain the incomplete depletion of STN1 in our model. First, the distance between the two *loxP* sites is ~5.5 kb. Since the Cre recombination efficiency is inversely proportional to the genetic distance between the *loxP* sites (*87*), it is possible that Cre recombination may be less robust in our system due to the relatively large distance between the two *loxP* sites. Second, Cre recombination is most effective in young mice <8 weeks old. Alteration of the treatment regimen to an earlier age of 4 weeks may increase the efficiency of deletion in vivo (*88*). Last, given the essential

role of CST in global DNA replication, it is possible that cells with efficient STN1 deletion halted growth and were outgrown by cells with decreased STN1 expression during tumor development.

Our initial investigation into the expression profile of DNA repair pathways in STN1$^{-/-}$ mice also showed high variation levels in non-BER genes including those in the FA pathway (FANCG, FANCI, and FANCF), MMR pathway (MSH3), and HR repair (INO80, MRE11, and RAD52) (table S1). However, when we tested their protein expression, these proteins were not down-regulated in STN1-deficient cells (fig. S7A). No MMC or cisplatin sensitivity was observed after STN1 depletion (fig. S7B), indicating that FA and HR pathways were minimally affected by STN1 deficiency. While we cannot exclude the possibility that other DNA repair pathways may be affected by STN1 reduction, our results suggest that the BER pathway was the most affected one. We also noticed that POLβ seems to be slighted elevated after STN1 knockdown (fig. S7A). The reason underlying this elevation is unknown. Since CST is an ssDNA-binding protein, it remains possible that CST might be involved in POLβ-mediated gap filling by binding to the ssDNA gap. Further studies are needed to determine whether STN1 deficiency could cause deregulation of gap filling.

Our finding that STN1 deficiency suppresses transcription of multiple genes in human and mammalian cells is somewhat unexpected. While future studies are needed to understand the mechanism underlying such regulation, our observation that STN1 deficiency slows down replication speed (Fig. 5C) leads us to favor the model that the slowed replication induces instabilities at the promoter regions of these genes that could adversely affect transcription machinery binding and/or elongation. One cause of this instability could be the transcription machinery collision with the slowed DNA replication machinery, which leads to RNA polymerase stalling and decreased transcription. Notably, previously, we have found that ~75% STN1 chromatin immunoprecipitation sequencing (ChIP-seq) peaks overlap with CpG islands and these sites are unstable under perturbed replication conditions (*35*). It is possible that the transcription machinery stalls at these regions upon STN1 deficiency. It has been reported that the budding yeast Cdc13-Stn1-Ten1 complex physically interacts with the transcription factor Spt5 and regulates RNA polymerase II transcription (*89*). The authors proposed that yeast CST may synchronize transcription with replication fork progression following head-on collision. Both our observation and the yeast findings suggest that CST may play a role in preventing replication/transcription collision to regulate gene expression.

Clinically, there has been much interest in telomere length and telomerase activity and its association with malignant transformation (*90*, *91*). Several studies indicated that CRCs display shorter telomeres when compared with the surrounding mucosa, especially in distant metastases (*92*–*94*). Telomere shortening can be accelerated by oxidative stress due to 8-oxoguanine formation at telomeres (*95*, *96*). CST has three distinct roles in telomere maintenance. It forms a complex with POT1-TPP1 (members of Shelterin) to inhibit telomerase activity from overextending the G-strand (*13*); it interacts with POLα during the late S-G_2 phase to initiate C-strand fill-in (*30*, *33*, *97*); it can directly melt G4 secondary structures that formed by tandem $(TTAGGG)_n$ repeats and thus prevents replication fork stalling and DNA gaps or breaks caused by G4 (*30*, *98*). Considering the role of CST in telomere maintenance along with our finding that STN1 down-regulation promotes oxidative stress, it is of interest to examine the effects of STN1 knockdown at telomeres. Our result shows that STN1 depletion induces an increase in telomere DNA damage; however, the level of telomere damage is low (less than five TIFs per cell), and the majority of DNA damage is at nontelomeric region (fig. S5). It is possible that this could be due to partial STN1 depletion in our model, or the effect on telomere shortening might require chronic exposure to oxidative damage. Nevertheless, we think that the global genome instability plays an important role in CRC tumorigenesis, especially during the initial phases of CRC, and telomere instability may further destabilize the genome and contribute to tumorigenesis.

For our CRC model, we used the AOM model rather than the more commonly used AOM/dextran sulfate sodium model of colitis-associated cancer (CAC). The rationale for this was that since STN1 reduction could potentially lead to bone marrow failure and thus affecting both innate and adaptive immune responses to gut inflammation, we wished to eliminate this possible complication from our study. Furthermore, AOM is a well-established model for CRC studies (*99*–*101*). Nevertheless, STN1 reduction in young adult mice did not affect body weight (Fig. 2D), did not result in alterations to the size of the spleen or lymph nodes, nor did it increase levels of bloody diarrhea compared with AOM-treated controls. Thus, our model will allow us to investigate whether STN1 deficiency promotes CAC in future studies.

Our results show that mammalian STN1 can influence proliferation and apoptosis in live animals. While more in-depth molecular studies are needed to pinpoint the exact mechanisms by which STN1 affects WNT, c-MYC, and COX-2, future clinical studies to determine whether STN1 can be used as a diagnostic marker will be valuable. Since STN1 deficiency leads to genome instability and gives rise to mutations that drive tumor development, this deficiency will affect the clinical outcome of cancer patient survival. Our data show that STN1-deficient cancer cells are more sensitive to DNA alkylating agents (Fig. 7B). Therefore, investigating the status of STN1 in CRC and other cancers may help physicians to select a more effective therapeutic strategy.

MATERIALS AND METHODS

Generation of STN1 cko mice and genotyping

The animals were housed and studied in specific pathogen–free animal facilities at Washington State University and Loyola University Chicago Health Sciences campuses. All studies were approved by Institutional Animal Care and Use Committees at both institutions. Wild-type (stock #000664) and *CreER*^{T2} C57BL/6 (stock #004682) strains were purchased from the Jackson Laboratory. To generate *STN1*$^{F/F}$ mice, the 3′ *loxP* was inserted to the exon 2 of *STN1* downstream of the ATG start codon, and the 5′ *loxP* was inserted ~5.5 kb upstream using CRISPR-Cas9 gene editing. Insertion sites were sequenced to ensure that no mutations were introduced. Founder mice were backcrossed to wild-type mice for at least five generations. *STN1*$^{F/F}$ mice were then crossed to *CreER*^{T2} to generate *CreER*^{T2};*STN1*$^{F/F}$ animals. All animals were weaned at 21 to 28 days old.

Genotyping of *STN1*$^{F/F}$ and *CreER*^{T2};*STN1*$^{F/F}$ mice was performed by polymerase chain reaction (PCR) using tail snip DNA. The primer sequences are listed in table S2. The *STN1*$^{F/F}$ allele was detected by PCR amplification of the 5′ *loxP* site with

primers 5′ wtF2 and 5′ mtR, yielding the PCR product of 547 base pairs (bp) for the floxed allele. The 3′ *loxP* site was amplified with primers 3′ mtF and 3′ wtR, yielding a 550-bp PCR product for the floxed allele. Genotyping of homozygous $STN1^{F/F}$ animals was performed with primers STN1loxPshift5′ and STN1loxPshift3′, yielding the PCR products of 218 bp for the floxed allele and 184 bp for the wild-type allele. For the above PCRs, thermocycling conditions consisted of one step of 5 min at 95°C, 30 cycles of 20 s at 95°C, 30 s at 60°C, and 40 s at 70°C, followed by 2 min at 72°C. Reactions contained 1 μl of tail lysate DNA, 0.75 mM primers, 100 mM deoxynucleotide triphosphates, 2.5 U of KOD Hot Start Polymerase (Sigma/Millipore), 2.5 mM $MgSO_4$, 0.5% dimethyl sulfoxide, and 10× PCR buffer in a total of 12.5-μl reaction. The $CreER^{T2}$ allele was detected following the PCR protocol provided by the Jackson Laboratory.

AOM inducing CRC in mice

Mice (8 weeks old) were administrated daily for five consecutive days with intraperitoneal injections of tamoxifen (APExBIO, 10540-29-1) in peanut oil (ACROS Organics, 8002-03-07) with approximately 100 mg/kg per injection. Two weeks following tamoxifen administration, animals were treated with AOM (Sigma-Aldrich, 25843-45-2) in sterilized phosphate-buffered saline (PBS) weekly for six consecutive weeks (approximately 12.5 mg/kg per injection, intraperitoneally). Mice were sacrificed 26 to 30 weeks after tamoxifen treatment for tissue collection. Twelve $STN1^{+/+}$ mice and 10 $STN1^{-/-}$ mice were treated, monitored, and analyzed at Washington State University by one research member, and the remaining nine $STN1^{+/+}$ mice and nine $STN1^{-/-}$ mice were treated, monitored, and analyzed at Loyola University Chicago by another research individual.

Tissue collection and histological examination

The entire colon was excised and opened longitudinally along the entire length, followed by an ice-cold PBS rinse to remove fecal pellets. The colon was further cut into three equal-length segments, representing proximal, medial, and distal portions. Each segment was further cut into two smaller portions. One-half of each segment was dipped into 10% buffered formalin phosphate (Fisher Chemical) for 72 hours at 4°C. Buffer was then removed, and the tissue was filled with 70% ethanol and kept at −20°C. The paraffin-embedded tissues were cut at 4-μm thickness and stained with hematoxylin and eosin for microscopic observation. The other half was immediately frozen in liquid nitrogen and kept at −80°C.

Western blotting

Frozen colon tissue was ground with a mortar and pestle precooled with liquid nitrogen, and the tissue powder was lysed with 1% CHAPS buffer on ice for 30 min. An equal amount of protein samples was subjected to 10% SDS–polyacrylamide gel electrophoresis for Western blot analysis. After protein transfer to polyvinylidene difluoride membrane (Millipore), the membrane was processed sequentially with anti-OBFC1/STN1 (Santa Cruz Biotechnology, sc-376450, RRID:AB_11149742) and anti-mouse immunoglobulin G (IgG) TrueBlot ULTRA Ig horseradish peroxidase (HRP) (Rockland, 18-8817-30, RRID:AB_2610849) to detect murine STN1.

Antibodies used for detecting DNA glycosylases and DNA repair proteins were anti-OGG1 (Santa Cruz Biotechnology, sc-376935), NEIL2 (GeneTex, GTX132565, RRID:AB_2886678), SMUG1 (AbClonal, A10166, RRID:AB_2757693), MPG (1:2000; ProteinTech, 67920-1-Ig, RRID:AB_2918672), POLβ (1:2000; ProteinTech, 18003-1-AP, RRID:AB_2299845), APEX1 (1:1000; ProteinTech, 10203-1-AP, RRID:AB_2057927), FANCG (1:1000; ProteinTech, 10215-1-AP, RRID:AB_2231541), FANCI (1:3000; ProteinTech, 20789-1-AP, RRID:AB_10694829), MSH3 (1:10,000; ProteinTech, 22393-1-AP, RRID:AB_11232405), RAD52 (1:5000; ProteinTech, 28045-1-AP, RRID:AB_2881046), INO80 (1:1000; ProteinTech, 18810-1-AP, RRID:AB_10598463), and MRE11 (1:1000; GeneTex, GTX70212, RRID:AB_372398). Glyceraldehyde-3-phosphate dehydrogenase (GAPDH) (1:10,000; Cell Signaling, 5174, RRID:AB_10622025) or β-actin (1:60,000; Sigma-Aldrich, A1978, RRID:AB_476692) was used as loading control. Anti-STN1 (1:100; Sigma-Aldrich, WH0079991M1, RRID:AB_1842768) and anti-CTC1 (1:1000; Abcam, ab230538) were used to detect human STN1 and CTC1 in HCT116 cells, respectively. Secondary antibodies were HRP-conjugated goat anti-rabbit IgG (1:1000; Vector Laboratories, PI-1000, RRID:AB_2336198) and HRP-conjugated anti-mouse IgG (1:1000; BD Biosciences, 554002, RRID:AB_395198).

IHC and TUNEL assay

Paraffin-embedded colon tissue sections from mice (4 μm) were dewaxed with xylene, and the sections were rehydrated in ethanol and then treated with 3% hydrogen peroxide. The sections were then immersed in target antigen retrieval buffer [10 mM tris base, 1 mM EDTA, and 0.05% Tween 20 (pH 9.0)], boiled for 10 min, then cooled down for 2 hours, and incubated with primary antibodies at 4°C overnight. The primary antibodies were anti-Cox2 (1:200; Bethyl, A303-600A, RRID:AB_11125751), anti–β-catenin (1:400; Bethyl, A700-086, RRID:AB_2891883), anti–c-Myc (Bethyl, A190-105A, RRID:AB_67390), anti-Ki67 (1:500; Life Technologies, MA5-14520, AB_10979488), and anti-γH2AX (1:500; Active Motif, 39117, RRID:AB_2793161). To detect STN1 in human tissue samples, unstained human colon carcinoma tissue arrays (OD-CT-DgCol01-005) were obtained from US Biomax Inc. and processed as described above. Anti-STN1 (1:100; Sigma-Aldrich, WH0079991M1) was used to detect hSTN1. Samples were then incubated with HRP-conjugated goat anti-rabbit IgG (1:1000; Vector Laboratories, PI-1000, RRID:AB_2336198) or HRP-conjugated anti-mouse IgG (1:1000; BD Biosciences, 554002, RRID:AB_395198) and stained using a DAB kit (Biotium, 30015). Last, samples were counterstained with hematoxylin. TUNEL assay was performed following the manufacturer′s instruction for embedded tissue section using the TUNEL Assay Kit (Abcam, ab206386). Images for IHC and TUNEL quantification were obtained under an EVOS XL Core microscope (Invitrogen) with a 20× objective. For all IHC staining and TUNEL assays, the paraffin-embedded distal colon tissues from four pairs of mice [$STN1^{+/+}$ (n = 4) versus $STN1^{-/-}$ (n = 4)] were processed for staining. Quantification of IHC signals was calculated using ImageJ. At least 5000 cells were counted in each group. Statistical analyses were performed using two-tailed t tests in GraphPad Prism.

Genomic DNA isolation

Genomic DNA was isolated from the paraffin-embedded or frozen colon tissue. For the paraffin-embedded tissue, the protocol was performed following the manufacturer′s instructions using the NucleoSpin DNA FFPE XS Kit (Macherey-Nagel, 740980.50). Total

DNA was quantified using a BioTek Synergy H1 NanoDrop reader (Agilent Technologies, Santa Clara, CA, USA). One microgram of total DNA of each sample was used for WES. Genomic DNA isolation from freshly frozen tissue was performed using the QIAamp DNA Mini Kit (Qiagen, 51304) following its instructions.

WES sequencing analyses, processing, and variant calling

FASTQ files were subjected to quality control with the FastQC tool (v0.11.9; www.bioinformatics.babraham.ac.uk/projects/fastqc/), and adapters were trimmed using TrimGalore (v0.6.6; www.bioinformatics.babraham.ac.uk/projects/trim_galore/). High-quality read pairs were mapped to reference genome mm10 using bwa-mem (v0.7.17) (*102*) under optimal parameter for pair-ended WES data followed by mark duplication using Picard tools (v2.26.0). The alignment file was then sorted and indexed using SAMtools (v1.11) (*103*). GATK toolkit (*104*–*106*) was used to perform base quality score recalibration and variant calling. GATK4 HaplotypeCaller and MuTect2 were used to call germline and somatic mutation, respectively. Hard filtering was then applied to raw variant data to extract high-confidence mutations.

Variant annotation and somatic signature profiling

High-confidence germline and somatic mutations were subjected to SNPeff (v5.0e) (*107*) to a gene-based and region-based annotation process. COSMIC SigProfiler (v3.2) (*108*) was used to identify somatic mutational processes by fitting the mutational signatures published in the COSMIC catalog (*109*) to the mutational profiles of the somatic mutations in each tumor. SigProfiler was performed using optimal options for mm10 WES data.

Cell culture

HCT116 was obtained from the American Type Culture Collection (CCL-247; RRID:CVCL_0291, Manassas, VA, USA) and passaged in Dulbecco's modified Eagle's medium (DMEM; GE Healthcare Life Sciences, Logan, UT, USA) supplemented with 10% cosmic calf serum (HyClone). MEF cells were isolated by harvesting embryos from pregnant mice 13 to 14 days after the formation of copulation plug and digesting the minced tissues with 0.25% trypsin-EDTA (*110*). MEF cells were grown in DMEM/F12 (Sigma-Aldrich) supplemented with 15% fetal bovine serum (Sigma-Aldrich), 50 μM β-mercaptoethanol (Sigma-Aldrich), and antibiotics (HyClone). All cells were grown at 37°C in a humidified atmosphere containing 5% CO_2. MEFs were then spontaneously immortalized after months of continued culturing and passaging.

Immunofluorescence staining

Immunofluorescence (IF) was carried out as described previously (*34*, *35*). Briefly, MEF cells (after 48 hours of 4-OHT treatment) or HCT116 cells (after shLUC or shSTN1 expression) were grown on chamber slides and then fixed directly with 4% paraformaldehyde (PFA) in PBS for 15 min at room temperature. Cells were then permeabilized with 0.15% Triton X-100 in PBS for 15 min, washed three times for 5 min with PBS, blocked with 10% bovine serum albumin (BSA) at 37°C for 1 hour in a humidified chamber, and then incubated with anti-γH2AX (1:1000, Active Motif, 39117) overnight at 4°C. After washing with PBS three times, slides were incubated with anti-rabbit DyLight 550 secondary antibody (Thermo Fisher Scientific, 84541, RRID:AB_10942173) at room temperature for 1 hour and washed three times in PBS. Slides were then dehydrated with cold ethanol series and dried in the dark. Nuclei were visualized by counterstaining with 4′,6-diamidino-2-phenylindole (DAPI) mounting medium (Vector Laboratories). Images were obtained under a Zeiss AxioImager M2 epifluorescence microscope with a 20× or 40× objective for quantification and representation.

γH2AX IF-telomere FISH

MEFs were grown in chamber slides and fixed in 4% PFA, followed by γH2AX immunostaining as described above. Slides were then refixed with 4% PFA for 10 min, dehydrated in 70, 85, and 100% ethanol, air-dried, and hybridized to Alexa Fluor 488–conjugated PNA telomere probe (Panagene). The slides were denatured for 5 min at 90°C, incubated for 2 hours at room temperature, and washed with 70% formamide in 10 mM tris (pH 7.5) for 15 min twice, followed by three times of wash in 0.1 M tris (pH 7.5)/0.15 M NaCl/0.08% Tween 20 for 5 min each. Slides were then dehydrated in ethanol series, DNA was counterstained with DAPI, and Z-stack images were taken at a 0.275-μm thickness per slice under a Zeiss AxioImager M2 epifluorescence microscope.

DNA fiber assay

MEF cells were first labeled with 25 μM CldU for 20 min and then washed and followed by addition of 250 μM IdU with or without AOM (1.25 μg/ml) for 40 min. Subsequently, cells were harvested, resuspended in PBS to 1000 cells/μl, and lysed in lysis buffer [200 mM tris-HCl (pH 7.4), 50 mM EDTA, and 0.5% SDS], and then DNA fibers were stretched on glass slides. Following fixation in methanol:acetic acid (3:1), slides were denatured with 2.5 M HCl for 80 min, washed with PBS, and then blocked with 5% BSA in PBS (w/v) for 30 min. Nascent DNA labeled by CIdU and IdU was immunostained with anti-CldU (Abcam, ab6326, RRID:AB_305426) and anti-IdU (BD Biosciences, 347580, RRID:AB_400326) antibodies and then incubated with anti-rat Alexa Fluor 488 (Thermo Fisher Scientific, A11006, RRID:AB_2534074) and anti-mouse Alexa Fluor 568 (Thermo Fisher Scientific, A11031, RRID:AB_144696) secondary antibodies. Coverslips were mounted using mounting medium (Vector Lab). Images were acquired with a Zeiss AxioImager M2 epifluorescence microscope at ×40 magnification and analyzed using the ImageJ software. Two independent treatments and fiber experiments were performed to ensure reproducibility. Results from one set of experiments are shown in the main figure.

RNA isolation and qPCR

Total RNA was isolated using TRIzol (Life Technologies Inc., 15596026) according to the manufacturer's protocol. Approximately 2 μg of RNA was used in the reverse transcription reaction using the First Strand cDNA Synthesis Kit (OriGene, 11801-025). Quantitative PCR (qPCR) was performed with 50 ng of cDNA, 1× Power SYBR Green PCR Master Mix (Life Technologies Inc., 4367659), and 10 pM of each primer in a total volume of 20 μl with the following thermal cycling setting: 2 min at 50°C, 10 min at 95°C for initial denaturation, and then followed by 40 cycles of 15 s at 95°C, 1 min at 60°C in QuantStudio 6 Flex (Life Technologies Inc.). Primer sequences for qPCR are shown in table S2. The mouse actin gene was used as the internal control. Relative quantification was calculated using the $2^{-\Delta\Delta Ct}$ method.

Alkaline comet assay

Cells were treated with or without AOM (1.25 μg/ml) in six-well plates for 30 min at 37°C. Immediately after treatment, cells were collected and suspended in 1× PBS to 500 cells/ml. Ten microliters of cell suspension was mixed with 90 μl of 1% low melting point agarose at 37°C, and 50 μl of mixture was spread onto a 1% normal agarose precoated Comet slide (R&D Systems, 4250-050-03). Cells were lysed by immersing the slides in a freshly prepared lysis solution [2.5 M NaCl, 100 mM EDTA, 10 mM tris base, 200 mM NaOH, 1% SDS, and 1% Triton X-100 (pH 10)] at 4°C in the dark for 1 hour. Slides were then removed from the lysis buffer and gently immersed in prechilled alkaline electrophoresis solution (AES) [200 mM NaOH and 1 mM disodium EDTA (pH 13)] at 4°C in the dark for 1 hour to allow DNA unwinding. Electrophoresis was subsequently performed at 20 V for 30 min at 4°C with prechilled AES. Following electrophoresis, slides were immersed twice in dH_2O and once in 70% ethanol for 5 min each at room temperature, dried at 37°C, and stained with 1× SYBR Gold solution (Thermo Fisher Scientific Inc.). Images were acquired with an epifluorescence microscope (Axio Imager M2; Zeiss AG, Oberkochen, Germany). Data were analyzed and presented in terms of % DNA in tail using ImageJ with the OpenComet plugin (*111*). At least 100 cells per sample were selected from random fields for quantification.

Oxidative DNA damage detection (Fpg comet assay)

MEF cells were collected and suspended in 1× PBS to 500 cells/ml. Ten microliters of cell suspension was mixed with 90 μl of 1% low melting point agarose at 37°C, and 50 μl of the mixture was spread onto a 1% normal agarose precoated Comet slide (R&D Systems, 4250-050-03). Cells were lysed by immersing the slides in a freshly prepared lysis solution [2.5 M NaCl, 100 mM EDTA, 10 mM tris base, 200 mM NaOH, 1% SDS, and 1% Triton X-100 (pH 10)] at 4°C in the dark for 1 hour, followed by treatment with 4 U of Fpg (New England Biolabs, M0240S) in NEB buffer 1 at 37°C for 30 min. Alkaline comet assay was then performed as described above.

AAG-APE1 comet assay

MEF cells were collected and suspended in 1× PBS to 500 cells/ml. Ten microliters of cell suspension was mixed with 90 μl of 1% low melting point agarose at 37°C, and 50 μl of the mixture was spread onto a 1% normal agarose precoated Comet slide. Cells were lysed by immersing slides in a freshly prepared lysis solution [2.5 M NaCl, 100 mM EDTA, 10 mM tris base, 200 mM NaOH, 1% SDS, and 1% Triton X-100 (pH 10)] at 4°C in the dark for 1 hour, followed by treatment with 10 U of hAAG (New England Biolabs, M0313S) in 1× NEB ThermoPol Reaction Buffer at 37°C for 1 hour. Slides were washed three times in PBS and immersed in 1× NEB buffer 4 for 15 min at room temperature, followed by treatment with 10 U of APE1 (New England Biolabs, M0282S) in 1× NEB buffer 4 at 37°C for 1 hour. Slides were then washed with PBS and gently immerse in prechilled neutral electrophoresis solution [NES; 100 mM tris base and 300 mM sodium acetate (pH 9.0)] at 4°C for 30 min. Electrophoresis was subsequently performed at 20 V for 30 min at 4°C with prechilled NES. Following electrophoresis, comet slides were sequentially immersed in DNA precipitation solution (1 M ammonium acetate and 85% ethanol) for 30 min at room temperature and 70% ethanol for 30 min at room temperature, dried at 37°C, and stained with 1× SYBR Gold solution (Thermo Fisher Scientific Inc.).

RNA interference

Small interference RNA (siRNA) sequences targeting human STN1 were described in our previous studies (*30*, *34*, *35*). siSTN1-1 targets GATCCTGTGTTTCTAGCCT, siSTN1-2/shSTN1-2 targets GCTT AACCTCACAACTTAA, shSTN1-4 targets GGACUGCCAGAAAC CAAAT of STN1, and shCTC1 targets GAAAGUCUUGUCC GGUAUU of CTC1 (*67*). HCT116 cells were transfected with siRNA oligos at a final concentration of 20 nM using Xtreme RNAi transfection reagent (Sigma-Aldrich) according to the manufacturer's protocol. Cells were collected 48 hours after transfection for Western blotting analysis. HCT116 cells expressing shSTN1 or shCTC1 were made by retroviral transduction followed by 4 days of puromycin selection. Control shRNA targeting luciferase was CG UACGCGGAAUACUUCGA (shLUC).

Colony formation assay

Eight hundred cells were seeded in six-well plates in triplicate 1 day before treatment. Cells were then treated with the indicated concentrations of MMS (Sigma-Aldrich), H_2O_2, cisplatin (Selleckchem), or MMC (Selleckchem) for 24 hours, or TMZ (Selleckchem) for 48 hours. Drugs were then removed from the medium. After 8 days of incubation, the medium was removed, and cells were fixed and stained with the crystal violet solution (0.1% crystal violet, 1% methanol, and 1% formaldehyde). Cell viability was calculated by normalizing the colony numbers of treated samples to untreated samples.

Survival data analysis

Survival curves were performed using cBioPortal with the data source TCGA CRC. Analysis results were performed with mRNA expression z-scores relative to all samples at threshold 2.0. $P < 0.05$ was considered as significant output.

Gene expression data analysis

The Wanderer portal (*112*) was used to examine *STN1* and *CTC1* gene expression in CRC patients with TCGA Pan-Cancer Atlas datasets in Fig. 1 (C to F). To examine the correlation between STN1 and BER glycosylase gene expression in human and mouse tissue samples, we used ChIPBase v2.0 portal (*113*) to analyze four datasets, including TCGA Pan-Cancer and GTEx dataset (*78*) for human samples and mouse tissue gene expression dataset (*79*, *80*).

Supplementary Materials

This PDF file includes:

Figs. S1 to S7
Tables S1 and S2

View/request a protocol for this paper from *Bio-protocol*.

REFERENCES AND NOTES

1. R. L. Siegel, K. D. Miller, H. E. Fuchs, A. Jemal, Cancer statistics, 2021. *CA Cancer J. Clin.* **71**, 7–33 (2021).
2. R. L. Siegel, S. A. Fedewa, W. F. Anderson, K. D. Miller, J. Ma, P. S. Rosenberg, A. Jemal, Colorectal cancer incidence patterns in the United States, 1974-2013. *J. Natl. Cancer Inst.* **109**, djw322 (2017).

3. S. Jones, W. D. Chen, G. Parmigiani, F. Diehl, N. Beerenwinkel, T. Antal, A. Traulsen, M. A. Nowak, C. Siegel, V. E. Velculescu, K. W. Kinzler, B. Vogelstein, J. Willis, S. D. Markowitz, Comparative lesion sequencing provides insights into tumor evolution. *Proc. Natl. Acad. Sci. U.S.A.* **105**, 4283–4288 (2008).
4. P. M. Heavey, D. McKenna, I. R. Rowland, Colorectal cancer and the relationship between genes and the environment. *Nutr. Cancer* **48**, 124–141 (2004).
5. J. Terzic, S. Grivennikov, E. Karin, M. Karin, Inflammation and colon cancer. *Gastroenterology* **138**, 2101–2114.e5 (2010).
6. American Cancer Society. Colorectal Cancer Facts & Figures 2020-2022. Atlanta: American Cancer Society (2020).
7. T. Armaghany, J. D. Wilson, Q. Chu, G. Mills, Genetic alterations in colorectal cancer. *Gastrointest. Cancer Res.* **5**, 19–27 (2012).
8. M. S. Pino, D. C. Chung, The chromosomal instability pathway in colon cancer. *Gastroenterology* **138**, 2059–2072 (2010).
9. A. C. F. Bolhaqueiro, B. Ponsioen, B. Bakker, S. J. Klaasen, E. Kucukkose, R. H. van Jaarsveld, J. Vivie, I. Verlaan-Klink, N. Hami, D. C. J. Spierings, N. Sasaki, D. Dutta, S. F. Boj, R. G. J. Vries, P. M. Lansdorp, M. van de Wetering, A. van Oudenaarden, H. Clevers, O. Kranenburg, F. Foijer, H. J. G. Snippert, G. J. P. L. Kops, Ongoing chromosomal instability and karyotype evolution in human colorectal cancer organoids. *Nat. Genet.* **51**, 824–834 (2019).
10. T. A. Knijnenburg, L. Wang, M. T. Zimmermann, N. Chambwe, G. F. Gao, A. D. Cherniack, H. Fan, H. Shen, G. P. Way, C. S. Greene, Y. Liu, R. Akbani, B. Feng, L. A. Donehower, C. Miller, Y. Shen, M. Karimi, H. Chen, P. Kim, P. Jia, E. Shinbrot, S. Zhang, J. Liu, H. Hu, M. H. Bailey, C. Yau, D. Wolf, Z. Zhao, J. N. Weinstein, L. Li, L. Ding, G. B. Mills, P. W. Laird, D. A. Wheeler, I. Shmulevich; Cancer Genome Atlas Research Network, R. J. Monnat Jr., Y. Xiao, C. Wang, Genomic and molecular landscape of dna damage repair deficiency across The Cancer Genome Atlas. *Cell Rep.* **23**, 239–254.e6 (2018).
11. L. H. Nguyen, A. Goel, D. C. Chung, Pathways of colorectal carcinogenesis. *Gastroenterology* **158**, 291–302 (2020).
12. N. M. Reilly, L. Novara, F. Di Nicolantonio, A. Bardelli, Exploiting DNA repair defects in colorectal cancer. *Mol. Oncol.* **13**, 681–700 (2019).
13. L. Y. Chen, S. Redon, J. Lingner, The human CST complex is a terminator of telomerase activity. *Nature* **488**, 540–544 (2012).
14. S. M. Noordermeer, S. Adam, D. Setiaputra, M. Barazas, S. J. Pettitt, A. K. Ling, M. Olivieri, A. Alvarez-Quilon, N. Moatti, M. Zimmermann, S. Annunziato, D. B. Krastev, F. Song, I. Brandsma, J. Frankum, R. Brough, A. Sherker, S. Landry, R. K. Szilard, M. M. Munro, A. McEwan, T. Goullet de Rugy, Z. Y. Lin, T. Hart, J. Moffat, A. C. Gingras, A. Martin, H. van Attikum, J. Jonkers, C. J. Lord, S. Rottenberg, D. Durocher, The shieldin complex mediates 53BP1-dependent DNA repair. *Nature* **560**, 117–121 (2018).
15. Y. V. Surovtseva, D. Churikov, K. A. Boltz, X. Song, J. C. Lamb, R. Warrington, K. Leehy, M. Heacock, C. M. Price, D. E. Shippen, Conserved telomere maintenance component 1 interacts with STN1 and maintains chromosome ends in higher eukaryotes. *Mol. Cell* **36**, 207–218 (2009).
16. J. A. Stewart, F. Wang, M. F. Chaiken, C. Kasbek, P. D. Chastain II, W. E. Wright, C. M. Price, Human CST promotes telomere duplex replication and general replication restart after fork stalling. *EMBO J.* **31**, 3537–3549 (2012).
17. P. Gu, J. N. Min, Y. Wang, C. Huang, T. Peng, W. Chai, S. Chang, CTC1 deletion results in defective telomere replication, leading to catastrophic telomere loss and stem cell exhaustion. *EMBO J.* **31**, 2309–2321 (2012).
18. Y. Miyake, M. Nakamura, A. Nabetani, S. Shimamura, M. Tamura, S. Yonehara, M. Saito, F. Ishikawa, RPA-like mammalian Ctc1-Stn1-Ten1 complex binds to single-stranded DNA and protects telomeres independently of the Pot1 pathway. *Mol. Cell* **36**, 193–206 (2009).
19. D. D. Nguyen, E. Y. Kim, P. B. Sang, W. Chai, Roles of OB-fold proteins in replication stress. *Front. Cell Dev. Biol.* **8**, 574466 (2020).
20. Y. Wang, W. Chai, Pathogenic CTC1 mutations cause global genome instabilities under replication stress. *Nucleic Acids Res.* **46**, 3981–3992 (2018).
21. K. H. Lei, H. L. Yang, H. Y. Chang, H. Y. Yeh, D. D. Nguyen, T. Y. Lee, X. Lyu, M. Chastain, W. Chai, H. W. Li, P. Chi, Crosstalk between CST and RPA regulates RAD51 activity during replication stress. *Nat. Commun.* **12**, 6412 (2021).
22. X. Lyu, P. B. Sang, W. Chai, CST in maintaining genome stability: Beyond telomeres. *DNA Repair (Amst.)* **102**, 103104 (2021).
23. B. H. Anderson, P. R. Kasher, J. Mayer, M. Szynkiewicz, E. M. Jenkinson, S. S. Bhaskar, J. E. Urquhart, S. B. Daly, J. E. Dickerson, J. O'Sullivan, E. O. Leibundgut, J. Muter, G. M. Abdel-Salem, R. Babul-Hirji, P. Baxter, A. Berger, L. Bonafe, J. E. Brunstom-Hernandez, J. A. Buckard, D. Chitayat, W. K. Chong, D. M. Cordelli, P. Ferreira, J. Fluss, E. H. Forrest, E. Franzoni, C. Garone, S. R. Hammans, G. Houge, I. Hughes, S. Jacquemont, P. Y. Jeannet, R. J. Jefferson, R. Kumar, G. Kutschke, S. Lundberg, C. M. Lourenco, R. Mehta, S. Naidu, K. K. Nischal, L. Nunes, K. Ounap, M. Philippart, P. Prabhakar, S. R. Risen, R. Schiffmann, C. Soh, J. B. Stephenson, H. Stewart, J. Stone, J. L. Tolmie, M. S. van der Knaap, J. P. Vieira, C. N. Vilain, E. L. Wakeling, V. Wermenbol, A. Whitney, S. C. Lovell, S. Meyer, J. H. Livingston, G. M. Baerlocher, G. C. Black, G. I. Rice, Y. J. Crow, Mutations in CTC1, encoding conserved telomere maintenance component 1, cause Coats plus. *Nat. Genet.* **44**, 338–342 (2012).
24. A. J. Simon, A. Lev, Y. Zhang, B. Weiss, A. Rylova, E. Eyal, N. Kol, O. Barel, K. Cesarkas, M. Soudack, N. Greenberg-Kushnir, M. Rhodes, D. L. Wiest, G. Schiby, I. Barshack, S. Katz, E. Pras, H. Poran, H. Reznik-Wolf, E. Ribakovsky, C. Simon, W. Hazou, Y. Sidi, A. Lahad, H. Katzir, S. Sagie, H. A. Aqeilan, G. Glousker, N. Amariglio, Y. Tzfati, S. Selig, G. Rechavi, R. Somech, Mutations in STN1 cause Coats plus syndrome and are associated with genomic and telomere defects. *J. Exp. Med.* **213**, 1429–1440 (2016).
25. E. Han, N. A. Patel, N. A. Yannuzzi, D. M. Laura, K. C. Fan, C. I. Negron, S. Prakhunhungsit, W. L. Thorson, A. M. Berrocal, A unique case of coats plus syndrome and dyskeratosis congenita in a patient with CTC1 mutations. *Ophthalmic Genet.* **41**, 363–367 (2020).
26. R. B. Keller, K. E. Gagne, G. N. Usmani, G. K. Asdourian, D. A. Williams, I. Hofmann, S. Agarwal, CTC1 mutations in a patient with dyskeratosis congenita. *Pediatr. Blood Cancer* **59**, 311–314 (2012).
27. S. Ganduri, N. F. Lue, STN1-POLA2 interaction provides a basis for primase-pol α stimulation by human STN1. *Nucleic Acids Res.* **45**, 9455–9466 (2017).
28. M. Goulian, C. J. Heard, The mechanism of action of an accessory protein for DNA polymerase alpha/primase. *J. Biol. Chem.* **265**, 13231–13239 (1990).
29. D. E. Casteel, S. Zhuang, Y. Zeng, F. W. Perrino, G. R. Boss, M. Goulian, R. B. Pilz, A DNA polymerase-α•primase cofactor with homology to replication protein A-32 regulates DNA replication in mammalian cells. *J. Biol. Chem.* **284**, 5807–5818 (2009).
30. C. Huang, X. Dai, W. Chai, Human Stn1 protects telomere integrity by promoting efficient lagging-strand synthesis at telomeres and mediating C-strand fill-in. *Cell Res.* **22**, 1681–1695 (2012).
31. N. F. Lue, J. Chan, W. E. Wright, J. Hurwitz, The CDC13-STN1-TEN1 complex stimulates Pol α activity by promoting RNA priming and primase-to-polymerase switch. *Nat. Commun.* **5**, 5762 (2014).
32. X. Feng, S. J. Hsu, A. Bhattacharjee, Y. Wang, J. Diao, C. M. Price, CTC1-STN1 terminates telomerase while STN1-TEN1 enables C-strand synthesis during telomere replication in colon cancer cells. *Nat. Commun.* **9**, 2827 (2018).
33. X. Dai, C. Huang, A. Bhusari, S. Sampathi, K. Schubert, W. Chai, Molecular steps of G-overhang generation at human telomeres and its function in chromosome end protection. *EMBO J.* **29**, 2788–2801 (2010).
34. X. Lyu, K. H. Lei, P. Biak Sang, O. Shiva, M. Chastain, P. Chi, W. Chai, Human CST complex protects stalled replication forks by directly blocking MRE11 degradation of nascent-strand DNA. *EMBO J.* **40**, e103654 (2021).
35. M. Chastain, Q. Zhou, O. Shiva, M. Fadri-Moskwik, L. Whitmore, P. Jia, X. Dai, C. Huang, P. Ye, W. Chai, Human CST facilitates genome-wide RAD51 recruitment to GC-rich repetitive sequences in response to replication stress. *Cell Rep.* **16**, 1300–1314 (2016).
36. M. Barazas, S. Annunziato, S. J. Pettitt, I. de Krijger, H. Ghezraoui, S. J. Roobol, C. Lutz, J. Frankum, F. F. Song, R. Brough, B. Evers, E. Gogola, J. Bhin, M. van de Ven, D. C. van Gent, J. J. L. Jacobs, R. Chapman, C. J. Lord, J. Jonkers, S. Rottenberg, The CST complex mediates end protection at double-strand breaks and promotes PARP inhibitor sensitivity in BRCA1-deficient cells. *Cell Rep.* **23**, 2107–2118 (2018).
37. A. Ray Chaudhuri, E. Callen, X. Ding, E. Gogola, A. A. Duarte, J. E. Lee, N. Wong, V. Lafarga, J. A. Calvo, N. J. Panzarino, S. John, A. Day, A. V. Crespo, B. Shen, L. M. Starnes, J. R. de Ruiter, J. A. Daniel, P. A. Konstantinopoulos, D. Cortez, S. B. Cantor, O. Fernandez-Capetillo, K. Ge, J. Jonkers, S. Rottenberg, S. K. Sharan, A. Nussenzweig, Replication fork stability confers chemoresistance in BRCA-deficient cells. *Nature* **535**, 382–387 (2016).
38. Z. Mirman, N. K. Sasi, A. King, J. R. Chapman, T. de Lange, 53BP1-shieldin-dependent DSB processing in BRCA1-deficient cells requires CST–Polα–primase fill-in synthesis. *Nat. Cell Biol.* **24**, 51–61 (2022).
39. Z. Mirman, F. Lottersberger, H. Takai, T. Kibe, Y. Gong, K. Takai, A. Bianchi, M. Zimmermann, D. Durocher, T. de Lange, 53BP1-RIF1-shieldin counteracts DSB resection through CST- and Polα-dependent fill-in. *Nature* **560**, 112–116 (2018).
40. G. A. Dos Santos, N. I. Viana, R. Pimenta, J. A. de Camargo, V. R. Guimaraes, P. Romao, P. Candido, V. Ghazarian, S. T. Reis, K. R. M. Leite, M. Srougi, Pan-cancer analysis reveals that CTC1-STN1-TEN1 (CST) complex may have a key position in oncology. *Cancer Genet.* **262–263**, 80–90 (2022).
41. L. Wang, T. Ma, W. Liu, H. Li, Z. Luo, X. Feng, Pan-cancer analyses identify the CTC1-STN1-TEN1 complex as a protective factor and predictive biomarker for immune checkpoint blockade in cancer. *Front. Genet.* **13**, 859617 (2022).
42. C. M. Phelan, K. B. Kuchenbaecker, J. P. Tyrer, S. P. Kar, K. Lawrenson, S. J. Winham, J. Dennis, A. Pirie, M. J. Riggan, G. Chornokur, M. A. Earp, P. C. Lyra Jr., J. M. Lee, S. Coetzee, J. Beesley, L. McGuffog, P. Soucy, E. Dicks, A. Lee, D. Barrowdale, J. Lecarpentier, G. Leslie, C. M. Aalfs, K. K. H. Aben, M. Adams, J. Adlard, I. L. Andrulis, H. Anton-Culver, N. Antonenkova; AOCS study group, G. Aravantinos, N. Arnold, B. K. Arun, B. Arver, J. Azzollini, J. Balmana, S. N. Banerjee, L. Barjhoux, R. B. Barkardottir, Y. Bean, M. W. Beckmann, A. Beeghly-Fadiel, J. Benitez, M. Bermisheva, M. Q. Bernardini, M. J. Birrer, L. Bjorge, A. Black, K. Blankstein, M. J. Blok, C. Bodelon, N. Bogdanova, A. Bojesen,

B. Bonanni, A. Borg, A. R. Bradbury, J. D. Brenton, C. Brewer, L. Brinton, P. Broberg, A. Brooks-Wilson, F. Bruinsma, J. Brunet, B. Buecher, R. Butzow, S. S. Buys, T. Caldes, M. A. Caligo, I. Campbell, R. Cannioto, M. E. Carney, T. Cescon, S. B. Chan, J. Chang-Claude, S. Chanock, X. Q. Chen, Y. E. Chiew, J. Chiquette, W. K. Chung, K. B. M. Claes, T. Conner, L. S. Cook, J. Cook, D. W. Cramer, J. M. Cunningham, A. A. D'Aloisio, M. B. Daly, F. Damiola, S. D. Damirovna, A. Dansonka-Mieszkowska, F. Dao, R. Davidson, A. DeFazio, C. Delnatte, K. F. Doheny, O. Diez, Y. C. Ding, J. A. Doherty, S. M. Domchek, C. M. Dorfling, T. Dork, L. Dossus, M. Duran, M. Durst, B. Dworniczak, D. Eccles, T. Edwards, R. Eeles, U. Eilber, B. Ejlertsen, A. B. Ekici, S. Ellis, M. Elvira, E. Study, K. H. Eng, C. Engel, D. G. Evans, P. A. Fasching, S. Ferguson, S. F. Ferrer, J. M. Flanagan, Z. C. Fogarty, R. T. Fortner, F. Fostira, W. D. Foulkes, G. Fountzilas, B. L. Fridley, T. M. Friebel, E. Friedman, D. Frost, P. A. Ganz, J. Garber, M. J. Garcia, V. Garcia-Barberan, A. Gehrig, G. S. Collaborators, A. Gentry-Maharaj, A. M. Gerdes, G. G. Giles, R. Glasspool, G. Glendon, A. K. Godwin, D. E. Goldgar, T. Goranova, M. Gore, M. H. Greene, J. Gronwald, S. Gruber, E. Hahnen, C. A. Haiman, N. Hakansson, U. Hamann, T. V. O. Hansen, P. A. Harrington, H. R. Harris, J. Hauke, H. Study, A. Hein, A. Henderson, M. A. T. Hildebrandt, P. Hillemanns, S. Hodgson, C. K. Hogdall, E. Hogdall, F. B. L. Hogervorst, H. Holland, M. J. Hooning, K. Hosking, R. Y. Huang, P. J. Hulick, J. Hung, D. J. Hunter, D. G. Huntsman, T. Huzarski, E. N. Imyanitov, C. Isaacs, E. S. Iversen, L. Izatt, A. Izquierdo, A. Jakubowska, P. James, R. Janavicius, M. Jernetz, A. Jensen, U. B. Jensen, E. M. John, S. Johnatty, M. E. Jones, P. Kannisto, B. Y. Karlan, A. Karnezis, K. Kast, K. C. Investigators, C. J. Kennedy, E. Khusnutdinova, L. A. Kiemeney, J. I. Kiiski, S. W. Kim, S. K. Kjaer, M. Kobel, R. K. Kopperud, T. A. Kruse, J. Kupryjanczyk, A. Kwong, Y. Laitman, D. Lambrechts, N. Larranaga, M. C. Larson, C. Lazaro, N. D. Le, L. Le Marchand, J. W. Lee, S. B. Lele, A. Leminen, D. Leroux, J. Lester, F. Lesueur, D. A. Levine, D. Liang, C. Liebrich, J. Lilyquist, L. Lipworth, J. Lissowska, K. H. Lu, J. Lubinnski, C. Luccarini, L. Lundvall, P. L. Mai, G. Mendoza-Fandino, S. Manoukian, L. Massuger, T. May, S. Mazoyer, J. N. McAlpine, V. McGuire, J. R. McLaughlin, I. McNeish, H. Meijers-Heijboer, A. Meindl, U. Menon, A. R. Mensenkamp, M. A. Merritt, R. L. Milne, G. Mitchell, F. Modugno, J. Moes-Sosnowska, M. Moffitt, M. Montagna, K. B. Moysich, A. M. Mulligan, J. Musinsky, K. L. Nathanson, L. Nedergaard, R. B. Ness, S. L. Neuhausen, H. Nevanlinna, D. Niederacher, R. L. Nussbaum, K. Odunsi, E. Olah, O. I. Olopade, H. Olsson, C. Olswold, D. M. O'Malley, K. R. Ong, N. C. Onland-Moret; OPAL study group, N. Orr, S. Orsulic, A. Osorio, D. Palli, L. Papi, T. W. Park-Simon, J. Paul, C. L. Pearce, I. S. Pedersen, P. H. M. Peeters, B. Peissel, A. Peixoto, T. Pejovic, L. M. Pelttari, J. B. Permuth, P. Peterlongo, L. Pezzani, G. Pfeiler, K. A. Phillips, M. Piedmonte, M. C. Pike, A. M. Piskorz, S. R. Poblete, T. Pocza, E. M. Poole, B. Poppe, M. E. Porteous, F. Prieur, D. Prokofyeva, E. Pugh, M. A. Pujana, P. Pujol, P. Radice, J. Rantala, C. Rappaport-Fuerhauser, G. Rennert, K. Rhiem, P. Rice, A. Richardson, M. Robson, G. C. Rodriguez, C. Rodriguez-Antona, J. Romm, M. A. Rookus, M. A. Rossing, J. H. Rothstein, A. Rudolph, I. B. Runnebaum, H. B. Salvesen, D. P. Sandler, M. J. Schoemaker, L. Senter, V. W. Setiawan, G. Severi, P. Sharma, T. Shelford, N. Siddiqui, L. E. Side, W. Sieh, C. F. Singer, H. Sobol, H. Song, M. C. Southey, A. B. Spurdle, Z. Stadler, D. Steinemann, D. Stoppa-Lyonnet, L. E. Sucheston-Campbell, G. Sukiennicki, R. Sutphen, C. Sutter, A. J. Swerdlow, C. I. Szabo, L. Szafron, Y. Y. Tan, J. A. Taylor, M. K. Tea, M. R. Teixeira, S. H. Teo, K. L. Terry, P. J. Thompson, L. C. V. Thomsen, D. L. Thull, L. Tihomirova, A. V. Tinker, M. Tischkowitz, S. Tognazzo, A. E. Toland, A. Tone, B. Trabert, R. C. Travis, A. Trichopoulou, N. Tung, S. S. Tworoger, A. M. van Altena, D. Van Den Berg, A. H. van der Hout, R. B. van der Luijt, M. Van Heetvelde, E. Van Nieuwenhuysen, E. J. van Rensburg, A. Vanderstichele, R. Varon-Mateeva, A. Vega, D. V. Edwards, I. Vergote, R. A. Vierkant, J. Vijai, A. Vratimos, L. Walker, C. Walsh, D. Wand, S. Wang-Gohrke, B. Wappenschmidt, P. M. Webb, C. R. Weinberg, J. N. Weitzel, N. Wentzensen, A. S. Whittemore, J. T. Wijnen, L. R. Wilkens, A. Wolk, M. Woo, X. Wu, A. H. Wu, H. Yang, D. Yannoukakos, A. Ziogas, K. K. Zorn, S. A. Narod, D. F. Easton, C. I. Amos, J. M. Schildkraut, S. J. Ramus, L. Ottini, M. T. Goodman, S. K. Park, L. E. Kelemen, H. A. Risch, M. Thomassen, K. Offit, J. Simard, R. K. Schmutzler, D. Hazelett, A. N. Monteiro, F. J. Couch, A. Berchuck, G. Chenevix-Trench, E. L. Goode, T. A. Sellers, S. A. Gayther, A. C. Antoniou, P. D. P. Pharoah, Identification of 12 new susceptibility loci for different histotypes of epithelial ovarian cancer. *Nat. Genet.* **49**, 680–691 (2017).

43. C. Li, Z. Zhao, J. Zhou, Y. Liu, H. Wang, X. Zhao, Relationship between the TERT, TNIP1 and OBFC1 genetic polymorphisms and susceptibility to colorectal cancer in Chinese Han population. *Oncotarget* **8**, 56932–56941 (2017).
44. J. Ojha, V. Codd, C. P. Nelson, N. J. Samani, I. V. Smirnov, N. R. Madsen, H. M. Hansen, A. J. de Smith, P. M. Bracci, J. K. Wiencke, M. R. Wrensch, J. L. Wiemels, K. M. Walsh; ENGAGE Consortium Telomere Group, Genetic Variation associated with longer telomere length increases risk of chronic lymphocytic leukemia. *Cancer Epidemiol. Biomarkers Prev.* **25**, 1043–1049 (2016).
45. J. Gudmundsson, G. Thorleifsson, J. K. Sigurdsson, L. Stefansdottir, J. G. Jonasson, S. A. Gudjonsson, D. F. Gudbjartsson, G. Masson, H. Johannsdottir, G. H. Halldorsson, S. N. Stacey, H. Helgason, P. Sulem, L. Senter, H. He, S. Liyanarachchi, M. D. Ringel, E. Aguillo, A. Panadero, E. Prats, A. Garcia-Castano, A. De Juan, F. Rivera, L. Xu, L. A. Kiemeney, G. I. Eyjolfsson, O. Sigurdardottir, I. Olafsson, H. Kristvinsson, R. T. Netea-Maier, T. Jonsson, J. I. Mayordomo, T. S. Plantinga, H. Hjartarson, J. Hrafnkelsson, E. M. Sturgis, U. Thorsteinsdottir, T. Rafnar, A. de la Chapelle, K. Stefansson, A genome-wide association study yields five novel thyroid cancer risk loci. *Nat. Commun.* **8**, 14517 (2017).
46. N. Valimaki, H. Kuisma, A. Pasanen, O. Heikinheimo, J. Sjoberg, R. Butzow, N. Sarvilinna, H. R. Heinonen, J. Tolvanen, S. Bramante, T. Tanskanen, J. Auvinen, O. Uimari, A. Alkodsi, R. Lehtonen, E. Kaasinen, K. Palin, L. A. Aaltonen, Genetic predisposition to uterine leiomyoma is determined by loci for genitourinary development and genome stability. *eLife* **7**, e37110 (2018).
47. D. L. Duffy, G. Zhu, X. Li, M. Sanna, M. M. Iles, L. C. Jacobs, D. M. Evans, S. Yazar, J. Beesley, M. H. Law, P. Kraft, A. Visconti, J. C. Taylor, F. Liu, M. J. Wright, A. K. Henders, L. Bowdler, D. Glass, M. A. Ikram, A. G. Uitterlinden, P. A. Madden, A. C. Heath, E. C. Nelson, A. C. Green, S. Chanock, J. H. Barrett, M. A. Brown, N. K. Hayward, S. MacGregor, R. A. Sturm, A. W. Hewitt; Melanoma GWAS Consortium, M. Kayser, D. J. Hunter, J. A. Newton Bishop, T. D. Spector, G. W. Montgomery, D. A. Mackey, G. D. Smith, T. E. Nijsten, D. T. Bishop, V. Bataille, M. Falchi, J. Han, N. G. Martin, Novel pleiotropic risk loci for melanoma and nevus density implicate multiple biological pathways. *Nat. Commun.* **9**, 4774 (2018).
48. E. Cerami, J. Gao, U. Dogrusoz, B. E. Gross, S. O. Sumer, B. A. Aksoy, A. Jacobsen, C. J. Byrne, M. L. Heuer, E. Larsson, Y. Antipin, B. Reva, A. P. Goldberg, C. Sander, N. Schultz, The cBio cancer genomics portal: An open platform for exploring multidimensional cancer genomics data. *Cancer Discov.* **2**, 401–404 (2012).
49. R. L. Johnson, J. C. Fleet, Animal models of colorectal cancer. *Cancer Metastasis Rev.* **32**, 39–61 (2013).
50. M. M. Taketo, W. Edelmann, Mouse models of colon cancer. *Gastroenterology* **136**, 780–798 (2009).
51. A. Bissahoyo, R. S. Pearsall, K. Hanlon, V. Amann, D. Hicks, V. L. Godfrey, D. W. Threadgill, Azoxymethane is a genetic background-dependent colorectal tumor initiator and promoter in mice: Effects of dose, route, and diet. *Toxicol. Sci.* **88**, 340–345 (2005).
52. M. Perse, A. Cerar, Morphological and molecular alterations in 1,2 dimethylhydrazine and azoxymethane induced colon carcinogenesis in rats. *J. Biomed. Biotechnol.* **2011**, 473964 (2011).
53. C. De Filippo, G. Caderni, M. Bazzicalupo, C. Briani, A. Giannini, M. Fazi, P. Dolara, Mutations of the Apc gene in experimental colorectal carcinogenesis induced by azoxymethane in F344 rats. *Br. J. Cancer* **77**, 2148–2151 (1998).
54. P. Singh, M. Velasco, R. Given, A. Varro, T. C. Wang, Progastrin expression predisposes mice to colon carcinomas and adenomas in response to a chemical carcinogen. *Gastroenterology* **119**, 162–171 (2000).
55. M. V. Sepporta, R. Fuccelli, P. Rosignoli, G. Ricci, M. Servili, R. Fabiani, Oleuropein prevents azoxymethane-induced colon crypt dysplasia and leukocytes DNA damage in A/J mice. *J. Med. Food* **19**, 983–989 (2016).
56. A. E. Bridges, S. Ramachandran, K. Tamizhmani, U. Parwal, A. Lester, P. Rajpurohit, D. S. Morera, S. L. Hasanali, P. Arjunan, R. N. Jedeja, N. Patel, P. M. Martin, H. Korkaya, N. Singh, S. Manicassamy, P. D. Prasad, V. B. Lokeshwar, B. L. Lokeshwar, V. Ganapathy, M. Thangaraju, RAD51AP1 loss attenuates colorectal cancer stem cell renewal and sensitizes to chemotherapy. *Mol. Cancer Res.* **19**, 1486–1497 (2021).
57. A. A. Vivona, B. Shpitz, A. Medline, W. R. Bruce, K. Hay, M. A. Ward, H. S. Stern, S. Gallinger, K-ras mutations in aberrant crypt foci, adenomas and adenocarcinomas during azoxymethane-induced colon carcinogenesis. *Carcinogenesis* **14**, 1777–1781 (1993).
58. M. Takahashi, S. Nakatsugi, T. Sugimura, K. Wakabayashi, Frequent mutations of the beta-catenin gene in mouse colon tumors induced by azoxymethane. *Carcinogenesis* **21**, 1117–1120 (2000).
59. M. Suzui, M. Okuno, T. Tanaka, H. Nakagama, H. Moriwaki, Enhanced colon carcinogenesis induced by azoxymethane in min mice occurs via a mechanism independent of beta-catenin mutation. *Cancer Lett.* **183**, 31–41 (2002).
60. Q. S. Wang, K. Guda, A. Papanikolaou, M. Dong, D. W. Rosenberg, Expression of transforming growth factor beta1 and its type II receptor in mouse colon tumors induced by azoxymethane. *Int. J. Oncol.* **17**, 551–558 (2000).
61. F. Wang, J. Stewart, C. M. Price, Human CST abundance determines recovery from diverse forms of DNA damage and replication stress. *Cell Cycle* **13**, 3488–3498 (2014).
62. M. De Robertis, E. Massi, M. L. Poeta, S. Carotti, S. Morini, L. Cecchetelli, E. Signori, V. M. Fazio, The AOM/DSS murine model for the study of colon carcinogenesis: From pathways to diagnosis and therapy studies. *J. Carcinog.* **10**, 9 (2011).
63. A. B. Sparks, P. J. Morin, B. Vogelstein, K. W. Kinzler, Mutational analysis of the APC/beta-catenin/Tcf pathway in colorectal cancer. *Cancer Res.* **58**, 1130–1134 (1998).
64. J. A. Han, J. I. Kim, P. P. Ongusaha, D. H. Hwang, L. R. Ballou, A. Mahale, S. A. Aaronson, S. W. Lee, P53-mediated induction of Cox-2 counteracts p53- or genotoxic stress-induced apoptosis. *EMBO J.* **21**, 5635–5644 (2002).
65. S. Ogino, K. Nosho, G. J. Kirkner, T. Kawasaki, J. A. Meyerhardt, M. Loda, E. L. Giovannucci, C. S. Fuchs, CpG island methylator phenotype, microsatellite instability, BRAF mutation and clinical outcome in colon cancer. *Gut* **58**, 90–96 (2009).

66. S. K. H. Li, A. Martin, Mismatch repair and colon cancer: Mechanisms and therapies explored. *Trends Mol. Med.* **22**, 274–289 (2016).
67. C. Huang, P. Jia, M. Chastain, O. Shiva, W. Chai, The human CTC1/STN1/TEN1 complex regulates telomere maintenance in ALT cancer cells. *Exp. Cell Res.* **355**, 95–104 (2017).
68. F. Wang, J. A. Stewart, C. Kasbek, Y. Zhao, W. E. Wright, C. M. Price, Human CST has independent functions during telomere duplex replication and C-strand fill-in. *Cell Rep.* **2**, 1096–1103 (2012).
69. S. M. Ackerson, C. I. Gable, J. A. Stewart, Human CTC1 promotes TopBP1 stability and CHK1 phosphorylation in response to telomere dysfunction and global replication stress. *Cell Cycle* **19**, 3491–3507 (2020).
70. P. Gu, S. Chang, Functional characterization of human CTC1 mutations reveals novel mechanisms responsible for the pathogenesis of the telomere disease Coats plus. *Aging Cell* **12**, 1100–1109 (2013).
71. L. B. Alexandrov, J. Kim, N. J. Haradhvala, M. N. Huang, A. W. T. Ng, Y. Wu, A. Boot, K. R. Covington, D. A. Gordenin, E. N. Bergstrom, S. M. A. Islam, N. Lopez-Bigas, L. J. Klimczak, J. R. McPherson, S. Morganella, R. Sabarinathan, D. A. Wheeler, V. Mustonen; PCAWG Mutational Signatures Working Group, G. Getz, S. G. Rozen, M. R. Stratton; PCAWG Consortium, The repertoire of mutational signatures in human cancer. *Nature* **578**, 94–101 (2020).
72. L. Riva, A. R. Pandiri, Y. R. Li, A. Droop, J. Hewinson, M. A. Quail, V. Iyer, R. Shepherd, R. A. Herbert, P. J. Campbell, R. C. Sills, L. B. Alexandrov, A. Balmain, D. J. Adams, The mutational signature profile of known and suspected human carcinogens in mice. *Nat. Genet.* **52**, 1189–1197 (2020).
73. Y.-A. Kim, D. Wojtowicz, R. Sarto Basso, I. Sason, W. Robinson, D. S. Hochbaum, M. D. M. Leiserson, R. Sharan, F. Vadin, T. M. Przytycka, Network-based approaches elucidate differences within APOBEC and clock-like signatures in breast cancer. *Genome Med.* **12**, 52 (2020).
74. F. Carini, M. Mazzola, F. Rappa, A. Jurjus, A. G. Geagea, S. Al Kattar, T. Bou-Assi, R. Jurjus, P. Damiani, A. Leone, G. Tomasello, Colorectal carcinogenesis: Role of oxidative stress and antioxidants. *Anticancer Res.* **37**, 4759–4766 (2017).
75. M. Perše, Oxidative stress in the pathogenesis of colorectal cancer: Cause or consequence? *Biomed. Res. Int.* **2013**, 725710 (2013).
76. P. Vodicka, M. Urbanova, P. Makovicky, K. Tomasova, M. Kroupa, R. Stetina, A. Opattova, K. Kostovcikova, A. Siskova, M. Schneiderova, V. Vymetalkova, L. Vodickova, Oxidative damage in sporadic colorectal cancer: Molecular mapping of base excision repair glycosylases in colorectal cancer patients. *Int. J. Mol. Sci.* **21**, 2473 (2020).
77. S. Wirtz, G. Nagel, L. Eshkind, M. F. Neurath, L. D. Samson, B. Kaina, Both base excision repair and O6-methylguanine-DNA methyltransferase protect against methylation-induced colon carcinogenesis. *Carcinogenesis* **31**, 2111–2117 (2010).
78. J. Vivian, A. A. Rao, F. A. Nothaft, C. Ketchum, J. Armstrong, A. Novak, J. Pfeil, J. Narkizian, A. D. Deran, A. Musselman-Brown, H. Schmidt, P. Amstutz, B. Craft, M. Goldman, K. Rosenbloom, M. Cline, B. O'Connor, M. Hanna, C. Birger, W. J. Kent, D. A. Patterson, A. D. Joseph, J. Zhu, S. Zaranek, G. Getz, D. Haussler, B. Paten, Toil enables reproducible, open source, big biomedical data analyses. *Nat. Biotechnol.* **35**, 314–316 (2017).
79. T. M. Keane, L. Goodstadt, P. Danecek, M. A. White, K. Wong, B. Yalcin, A. Heger, A. Agam, G. Slater, M. Goodson, N. A. Furlotte, E. Eskin, C. Nellaker, H. Whitley, J. Cleak, D. Janowitz, P. Hernandez-Pliego, A. Edwards, T. G. Belgard, P. L. Oliver, R. E. McIntyre, A. Bhomra, J. Nicod, X. Gan, W. Yuan, L. van der Weyden, C. A. Steward, S. Bala, J. Stalker, R. Mott, R. Durbin, I. J. Jackson, A. Czechanski, J. A. Guerra-Assuncao, L. R. Donahue, L. G. Reinholdt, B. A. Payseur, C. P. Ponting, E. Birney, J. Flint, D. J. Adams, Mouse genomic variation and its effect on phenotypes and gene regulation. *Nature* **477**, 289–294 (2011).
80. R. Petryszak, M. Keays, Y. A. Tang, N. A. Fonseca, E. Barrera, T. Burdett, A. Fullgrabe, A. M. Fuentes, S. Jupp, S. Koskinen, O. Mannion, L. Huerta, K. Megy, C. Snow, E. Williams, M. Barzine, E. Hastings, H. Weisser, J. Wright, P. Jaiswal, W. Huber, J. Choudhary, H. E. Parkinson, A. Brazma, Expression Atlas update—An integrated database of gene and protein expression in humans, animals and plants. *Nucleic Acids Res.* **44**, D746–D752 (2016).
81. G. Bridge, S. Rashid, S. A. Martin, DNA mismatch repair and oxidative DNA damage: Implications for cancer biology and treatment. *Cancers (Basel)* **6**, 1597–1614 (2014).
82. J. Tchou, V. Bodepudi, S. Shibutani, I. Antoshechkin, J. Miller, A. P. Grollman, F. Johnson, Substrate specificity of Fpg protein. Recognition and cleavage of oxidatively damaged DNA. *J. Biol. Chem.* **269**, 15318–15324 (1994).
83. A. Hartwig, H. Dally, R. Schlepegrell, Sensitive analysis of oxidative DNA damage in mammalian cells: Use of the bacterial Fpg protein in combination with alkaline unwinding. *Toxicol. Lett.* **88**, 85–90 (1996).
84. L. Schomacher, D. Han, M. U. Musheev, K. Arab, S. Kienhöfer, A. von Seggern, C. Niehrs, Neil DNA glycosylases promote substrate turnover by Tdg during DNA demethylation. *Nat. Struct. Mol. Biol.* **23**, 116–124 (2016).
85. Z. Jiang, Y. Lai, J. M. Beaver, P. S. Tsegay, M. L. Zhao, J. K. Horton, M. Zamora, H. L. Rein, F. Miralles, M. Shaver, J. D. Hutcheson, I. Agoulnik, S. H. Wilson, Y. Liu, Oxidative DNA damage modulates DNA methylation pattern in human breast cancer 1 (BRCA1) gene via the crosstalk between DNA polymerase β and a de novo DNA methyltransferase. *Cell* **9**, 225 (2020).
86. Y. Li, P. Mao, E. Y. Basenko, Z. Lewis, M. J. Smerdon, W. Czaja, Versatile cell-based assay for measuring DNA alkylation damage and its repair. *Sci. Rep.* **11**, 18393 (2021).
87. B. Zheng, M. Sage, E. A. Sheppeard, V. Jurecic, A. Bradley, Engineering mouse chromosomes with Cre-loxP: Range, efficiency, and somatic applications. *Mol. Cell. Biol.* **20**, 648–655 (2000).
88. S. Feil, N. Valtcheva, R. Feil, Inducible Cre mice. *Methods Mol. Biol.* **530**, 343–363 (2009).
89. O. Calvo, N. Grandin, A. Jordán-Pla, E. Miñambres, N. González-Polo, J. E. Pérez-Ortín, M. Charbonneau, The telomeric Cdc13-Stn1-Ten1 complex regulates RNA polymerase II transcription. *Nucleic Acids Res.* **47**, 6250–6268 (2019).
90. C. B. Harley, Telomerase and cancer therapeutics. *Nat. Rev. Cancer* **8**, 167–179 (2008).
91. P. Aghagolzadeh, R. Radpour, New trends in molecular and cellular biomarker discovery for colorectal cancer. *World J. Gastroenterol.* **22**, 5678–5693 (2016).
92. R. Gertler, R. Rosenberg, D. Stricker, J. Friederichs, A. Hoos, M. Werner, K. Ulm, B. Holzmann, H. Nekarda, J. R. Siewert, Telomere length and human telomerase reverse transcriptase expression as markers for progression and prognosis of colorectal carcinoma. *J. Clin. Oncol.* **22**, 1807–1814 (2004).
93. X. Ye, J. Li, C. Song, W. Chen, Telomere in colorectal cancer associated with distant metastases and predicted a poor prognosis. *Transl. Cancer Res.* **10**, 2906–2917 (2021).
94. M. G. Kibriya, M. Raza, M. Kamal, Z. Haq, R. Paul, A. Mareczko, B. L. Pierce, H. Ahsan, F. Jasmine, Relative telomere length change in colorectal carcinoma and its association with tumor characteristics, gene expression and microsatellite instability. *Cancers (Basel)* **14**, 2250 (2022).
95. E. Fouquerel, R. P. Barnes, S. Uttam, S. C. Watkins, M. P. Bruchez, P. L. Opresko, Targeted and persistent 8-oxoguanine base damage at telomeres promotes telomere loss and crisis. *Mol. Cell* **75**, 117–130.e6 (2019).
96. M. De Rosa, S. A. Johnson, P. L. Opresko, Roles for the 8-oxoguanine DNA repair system in protecting telomeres from oxidative stress. *Front. Cell Dev. Biol.* **9**, 758402 (2021).
97. X. Feng, S. J. Hsu, C. Kasbek, M. Chaiken, C. M. Price, CTC1-mediated C-strand fill-in is an essential step in telomere length maintenance. *Nucleic Acids Res.* **45**, 4281–4293 (2017).
98. A. Bhattacharjee, Y. Wang, J. Diao, C. M. Price, Dynamic DNA binding, junction recognition and G4 melting activity underlie the telomeric and genome-wide roles of human CST. *Nucleic Acids Res.* **45**, 12311–12324 (2017).
99. M. Gerling, R. Glauben, J. K. Habermann, A. A. Kuhl, C. Loddenkemper, H. A. Lehr, M. Zeitz, B. Siegmund, Characterization of chromosomal instability in murine colitis-associated colorectal cancer. *PLOS ONE* **6**, e22114 (2011).
100. T. Kuno, Y. Hatano, H. Tomita, A. Hara, Y. Hirose, A. Hirata, H. Mori, M. Terasaki, S. Masuda, T. Tanaka, Organomagnesium suppresses inflammation-associated colon carcinogenesis in male Crj: CD-1 mice. *Carcinogenesis* **34**, 361–369 (2013).
101. C. Luceri, C. De Filippo, G. Caderni, L. Gambacciani, M. Salvadori, A. Giannini, P. Dolara, Detection of somatic DNA alterations in azoxymethane-induced F344 rat colon tumors by random amplified polymorphic DNA analysis. *Carcinogenesis* **21**, 1753–1756 (2000).
102. H. Li, R. Durbin, Fast and accurate short read alignment with Burrows-Wheeler transform. *Bioinformatics* **25**, 1754–1760 (2009).
103. H. Li, B. Handsaker, A. Wysoker, T. Fennell, J. Ruan, N. Homer, G. Marth, G. Abecasis, R. Durbin; 1000 Genome Project Data Processing Subgroup, The sequence alignment/map format and SAMtools. *Bioinformatics* **25**, 2078–2079 (2009).
104. P. Danecek, A. Auton, G. Abecasis, C. A. Albers, E. Banks, M. A. DePristo, R. E. Handsaker, G. Lunter, G. T. Marth, S. T. Sherry, G. McVean, R. Durbin; 1000 Genomes Project Analysis Group, The variant call format and VCFtools. *Bioinformatics* **27**, 2156–2158 (2011).
105. A. McKenna, M. Hanna, E. Banks, A. Sivachenko, K. Cibulskis, A. Kernytsky, K. Garimella, D. Altshuler, S. Gabriel, M. Daly, M. A. DePristo, The Genome Analysis Toolkit: A MapReduce framework for analyzing next-generation DNA sequencing data. *Genome Res.* **20**, 1297–1303 (2010).
106. G. A. Van der Auwera, M. O. Carneiro, C. Hartl, R. Poplin, G. Del Angel, A. Levy-Moonshine, T. Jordan, K. Shakir, D. Roazen, J. Thibault, E. Banks, K. V. Garimella, D. Altshuler, S. Gabriel, M. A. DePristo, From FastQ data to high confidence variant calls: The Genome Analysis Toolkit best practices pipeline. *Curr. Protoc. Bioinformatics* **43**, 11.10.1–11.10.33 (2013).
107. P. Cingolani, A. Platts, L. L. Wang, M. Coon, T. Nguyen, L. Wang, S. J. Land, X. Lu, D. M. Ruden, A program for annotating and predicting the effects of single nucleotide polymorphisms, SnpEff: SNPs in the genome of *Drosophila melanogaster* strain w^{1118}; iso-2; iso-3. *Fly (Austin)* **6**, 80–92 (2012).
108. E. N. Bergstrom, M. N. Huang, U. Mahto, M. Barnes, M. R. Stratton, S. G. Rozen, L. B. Alexandrov, SigProfilerMatrixGenerator: A tool for visualizing and exploring patterns of small mutational events. *BMC Genomics* **20**, 685 (2019).
109. J. G. Tate, S. Bamford, H. C. Jubb, Z. Sondka, D. M. Beare, N. Bindal, H. Boutselakis, C. G. Cole, C. Creatore, E. Dawson, P. Fish, B. Harsha, C. Hathaway, S. C. Jupe, C. Y. Kok,

K. Noble, L. Ponting, C. C. Ramshaw, C. E. Rye, H. E. Speedy, R. Stefancsik, S. L. Thompson, S. Wang, S. Ward, P. J. Campbell, S. A. Forbes, COSMIC: The catalogue of somatic mutations in cancer. *Nucleic Acids Res.* **47**, D941–D947 (2019).

110. M. E. Durkin, X. Qian, N. C. Popescu, D. R. Lowy, Isolation of mouse embryo fibroblasts. *Bio Protoc.* **3**, e908 (2013).
111. B. M. Gyori, G. Venkatachalam, P. S. Thiagarajan, D. Hsu, M. V. Clement, OpenComet: An automated tool for comet assay image analysis. *Redox Biol.* **2**, 457–465 (2014).
112. A. Diez-Villanueva, I. Mallona, M. A. Peinado, Wanderer, an interactive viewer to explore DNA methylation and gene expression data in human cancer. *Epigenetics Chromatin* **8**, 22 (2015).
113. K. R. Zhou, S. Liu, W. J. Sun, L. L. Zheng, H. Zhou, J. H. Yang, L. H. Qu, ChIPBase v2.0: Decoding transcriptional regulatory networks of non-coding RNAs and protein-coding genes from ChIP-seq data. *Nucleic Acids Res.* **45**, D43–D50 (2017).

Acknowledgments: We thank E. Everson and S. Knowles for technical help, L. Zheng for discussing cko strategy, and Y. Liu for sharing the Fpg protocol. **Funding:** Research in Chai laboratory is supported by NIH R01CA234266 and R21ES034636 to W.C. The funding bodies had no role in study design, data collection, data analysis, and interpretation of data and in writing the manuscript. **Author contributions:** D.D.N., E.K., and W.C. designed the experiments. D.D.N. performed the majority of in vitro experiments, treated/monitored/collected tissues and data from 18 animals, performed all IHC experiments, analyzed TCGA and gene expression data, and assembled figures. E.K. established the animal colonies, isolated MEFs, optimized tamoxifen and AOM treatment conditions, and treated/monitored/collected tissues and data from 22 animals. N.T.L. and M.T.L. performed WES analysis. X.D. performed pathology analysis. R.K.J. performed RNAi in HCT116 and Western blotting. R.J.K. performed MMS sensitivity assay. T.N.T.N. participated in animal breeding/care, genotyping, and tissue Western blotting. O.S. performed genotyping and provided animal care. W.C. conceived and supervised the study and participated in various experiments. D.D.N., E.K., and W.C. wrote the manuscript with the help from M.T.L. **Competing interests:** The authors declare that they have no competing interests. **Data and materials availability:** WES data availability: NCBI BioProject—accession number PRJNA932280. Code availability: https://doi.org/10.5281/zenodo.7653103, DOI: 10.5281/zenodo.7653103. All data needed to evaluate the conclusions in the paper are present in the paper and/or the Supplementary Materials.

Submitted 20 September 2022
Accepted 5 April 2023
Published 10 May 2023
10.1126/sciadv.add8023